Conjugated polymer-based oxygen-sensitive luminescent nanoparticles

by

Shiwen Sun

Chemical and Biochemical Engineering Department,
Rutgers, the State University of New Jersey, USA

A scientific report submitted to Austrian Marshall Plan Foundation

Written under the direction of

Dr. Ingo Klimant

Dr. Sergey M. Borisov

Institute of Analytical Chemistry and Food Chemistry
Graz University of Technology, Austria

New Brunswick, New Jersey

March, 2014

Abstract

In this work, a series of new optical oxygen nanoparticle-based sensors were developed. The luminescent oxygen indicator dyes Pt(II)–5,15-di(pentafluorophenyl)-10,20-di(4-bromophenyl)porphyrin (PtTFPP), and Pt(II) meso-tetra(4-bromophenyl)tetra(tert-butyl)benzoporphyrin (PtTPTtBuBP) were covalently immobilized into two different conjugated polymers. The resulted polymers were rendered positively or negatively charged via chemical modification and were used to prepare oxygen-sensitive nanoparticles via nanoprecipitation technique.

Compared with indicator embedded or doped in polymer matrix, this method improved the brightness of oxygen sensor by 4-6 times. Efficient energy transfer was established from conjugated polymers to oxygen indicator dye. Highly efficient two-photon excitation is expected. Different functional groups were also added to achieve adequate stability in aqueous dispersion and cell-penetration ability for different types of cells and tissues. Further investigation is ongoing in Dr. Dmitri Papkovsky's group at University College Cork (Ireland).

Acknowledgement

First, I would like to express my sincere gratitude to Univ.-Prof. Dipl.-Chem. Dr.rer.nat. Ingo Klimant for having me as an exchange scholar to do research in his group. Even I only stayed for a short period, I still felt the warmness of his welcome and having me as a group member at Institute of Analytical Chemistry and Food Chemistry. Also, I couldn't have this research work and report done without Dr. Sergey Borisov. It is never too much to say "Thank you" once again to him for his continuous support, guidance, and help in every possible way. I deeply appreciate his wisdom, patience, and kindness. I have learned a lot from his immense knowledge, optimism and enthusiasm.

I never expected to have such a wonderful group to work with. I want to mention each of their names to express my thanks. We were not only working together as colleagues, but also learning from each other and sharing life stories as friends. I am so glad that we went through together from Sturm season to Glühwein season, filled up with different kinds of Schanpps in between. As we talked before, you are more than welcome to visit me no matter where I am.

Furthermore, I would like to thank Mag. Kathrin Manninger, Karin leber, and all the other beautiful ladies from International Relations and Mobility Programmes at TU Graz. It's you to make this happened and let me have my life easier in a foreign country. Also, thanks to Dr. Yee

I would like to thank Marshall Plan Scholarship Austria for financial support.

Last but not least, I would like to thank my parents and family for continuously supporting me and encouraging me to chase my dreams over the past years.

Contents

1 Introduction

Oxygen is one of the most important chemical species on the earth, especially for human beings. Quantitative determination of oxygen content, both in gas[1] and liquid phase[2], is of great importance for various fields, for example medicine, biology, food manufacturing, oceanography, environmental monitoring, etc.[3]. Based on different measuring methods, oxygen sensors can be divided into three categories: electrochemical[4], optical[5-7], and chemical (Winkler titration[8]).

Optical oxygen sensor received great attention recently due to its advantages over other methods: inexpensive, easily miniaturized, simple preparation, no electrical interference, and not oxygen consuming[5]. The major principle used for optical oxygen sensor is the quenching of the luminescence of an indicator dye by molecular oxygen[9]. The typical layout for an optical oxygen sensor consists of a luminescent indicator dye immobilized in a polymeric matrix, and deposited on a solid support (planar waveguide, microtitre plate, or optical fiber)[10].

The application area is also a critical factor for the design of optical oxygen sensors. In recent years, a great attention has been focused on the understanding of cellular function and processes taking place in both normal and abnormal cells and tissues[11]. In biological system, oxygen, as a small gaseous analyte, diffuses fast in solution, in and out of the cell, and is present in vast excess in the environment[12]. Therefore, it raises the demand the development of an accurate oxygen sensor which is versatile, flexible and simple. To satisfy these requirement, the “perfect” sensor should have high brightness, ability for cell penetration, be suitable for ratiometric two-wavelength measurement, potential for two-photon absorption, simple preparation and low

working concentrations. Several kinds of particle based cellular/ intracellular oxygen sensors have been presented by scientists [12-17], which met some of the requirement.

In this work, we present a series of conjugated polymer-based oxygen-sensitive nanoparticles, with high brightness, under dual emission for ratiometric measurement, functional groups for water dispersibility and cell penetration.

2 Theoretical background

2.1 Luminescence

The emission of photons from an electronically excited species is called luminescence. The luminescence compounds can be organic, inorganic, or organometallic compounds. Also, luminescence can be caused by many environmental influences. Various kinds of luminescence are classified by different modes of excitation (see Table 2.1)[18].

Table 2.1. The various types of luminescence

Type of luminescence	**Mode of excitation**
Photoluminescence (fluorescence, phosphorescence, delayed fluorescence)	Absorption of light (photons)
Electroluminescence	Electric field
Thermoluminescence	Heating after prior storage of energy
Chemiluminescence	Chemical process (e.g. oxidation)
Bioluminescence	Biochemical process

2.1.1 Absorption

With the absorption of photons, a luminescent molecule can be excited from its ground state (S_0) to a higher energy level, either the first or the second electronic state (S_1 or S_2)[10]. The energy difference between these two states is equal to the energy of photons absorbed. This transition is

fast, which takes place in about 10^{-15} s. The followed possible de-excitation processes can in illustrated by the Perrin–Jablonski diagram in Figure 2.1.

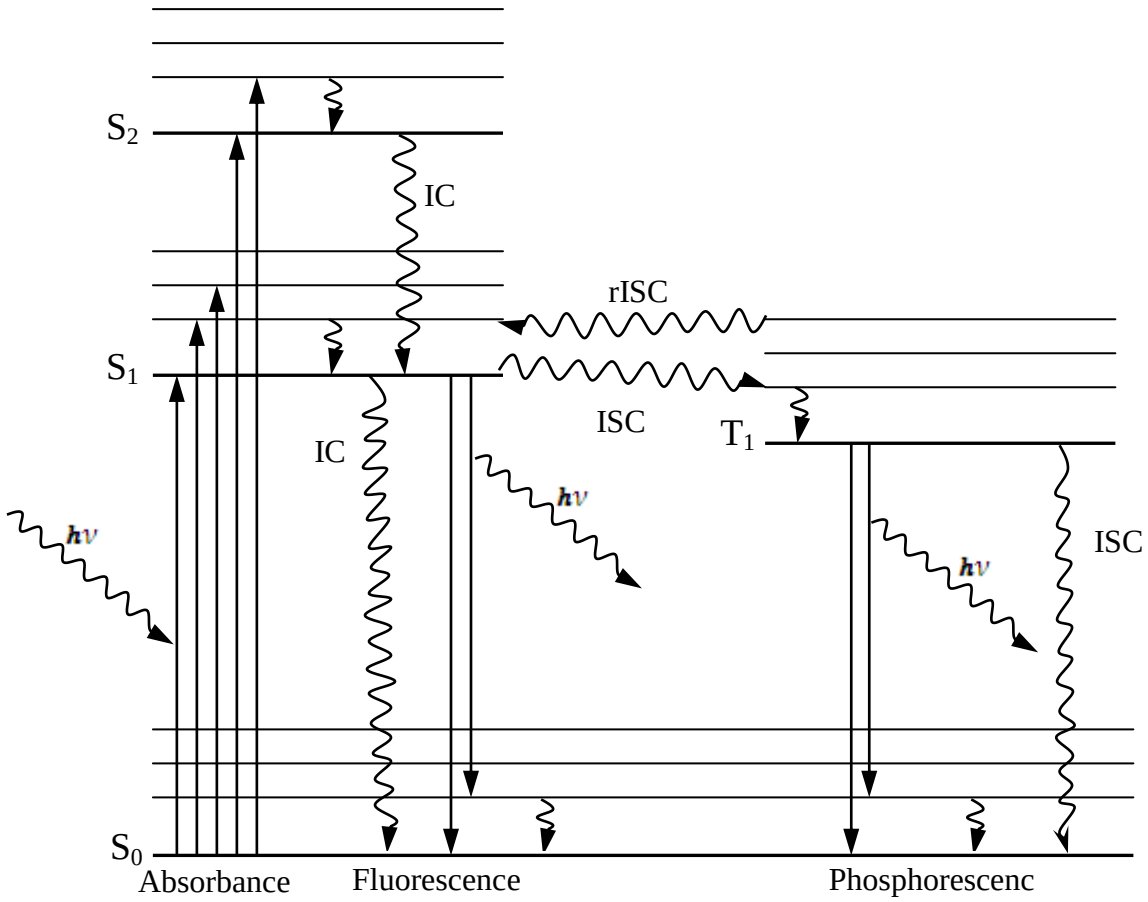

Figure 2.1. Perrin-Jablonski diagram.

Usually, the energy of these electronic transitions follows the order:

$$n \rightarrow \pi^* < \pi \rightarrow \pi^* < n \rightarrow \sigma^* < \sigma \rightarrow \sigma^*$$

In absorption and fluorescence spectroscopy, there are two important types of orbitals needed to be mentioned: the Highest Occupied Molecular Orbitals (HOMO) and the Lowest Unoccupied Molecular Orbitals (LUMO). Both HOMO and LUMO refer to the ground state of the molecule.

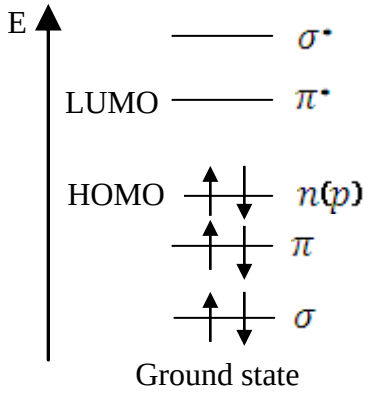

Figure 2.2. Energy levels of molecular orbitals in formaldehyde.

An example of energy level of formaldehyde in Figure 2.2, the HOMO is the n orbital and the LUMO is the π^* orbital. Mostly, two types of electronic transition occur during the absorption of visible light: $\pi \rightarrow \pi^*$ or $n \rightarrow \pi^*$. Because other electronic transitions occur at a higher energy level, thus need shorter wavelength of the corresponding absorption[18].

In most cases, the absorbance of a sample follows the *Beer-Lambert Law* (Eq.2-1).

$$A(\lambda) = \frac{\log\left(I_\lambda^0\right)}{I_\lambda} = \varepsilon(\lambda) l c \qquad \text{Eq. 2-1}$$

$A(\lambda)$	Absorption
I_λ^0	Intensity of light entering the sample
I_λ	Light intensity after passing through the sample
$\varepsilon(\lambda)$	Molar absorption coefficient of the dye at a certain wavelength λ ($M^{-1}cm^{-1}$)
l	optical path length of the sample
c	dye concentration (M)

2.1.2 The Frank-Condon principle

According to the Born-Oppenheimer approximation, the motions of electrons are much faster than the motions of the nuclei. The excitation of an electron to a higher lying unoccupied molecular orbital occurs in about 10^{-15} s. Meantime, the characteristic time for molecular vibrations is 10^{-10} – 10^{-12}s, which is slower. Based on this observation, we have the Frank-Condon principle: an electronic transition is most likely to occur without changes in the positions of the nuclei in the molecular entity and it environment. Consequently, the state is called Frank-Condon state, and the transition is called vertical transition. Therefore, we have the relation between the potential energy verse the nuclear configuration fitted in a Morse function[18] (see figure 2.3.).

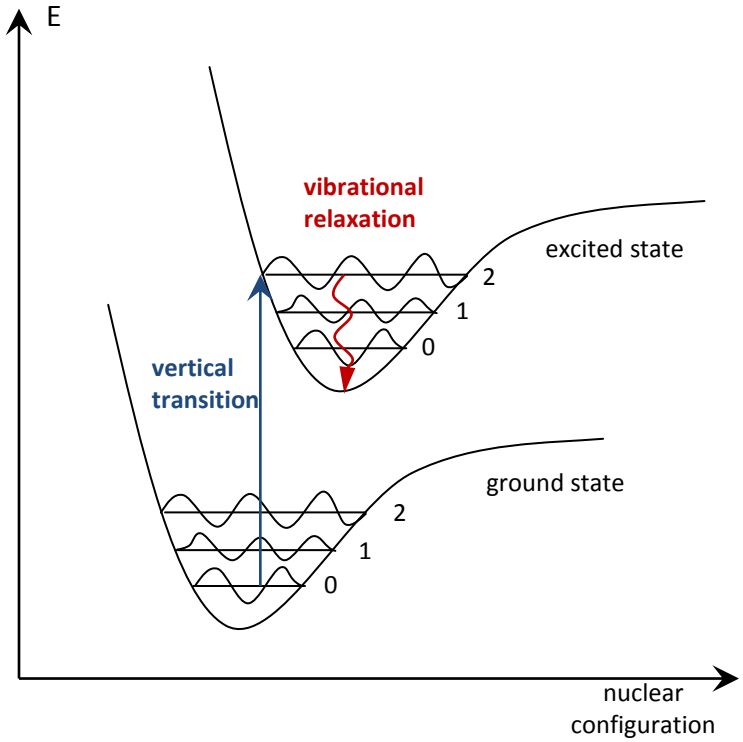

Figure 2.3. Frank-Condon principle.

2.1.3 Internal conversion

Internal conversion is a non-radiative transition of two electronic states with same spin multiplicity. Usually, in solution, a vibrational relaxation to vibrational ground state is followed. The extra energy can be released to the solution through the collisions of the surrounding solvent molecules with the excited molecules.

Internal conversion can take place only when it is more efficient than other energy transfer processes. For example, when a molecule has been excited to an energy level which is higher than the lowest vibrational level of S1, the excited molecule drops to the vibrational ground level within 10^{-13} – 10^{-11} s (see figure 2.4.). But the energy gap between S_1 to S_0 is larger than it between S_2 to S_1, so the internal conversion is not referred. Also, an excited molecule can remain in S_1 state for 10^{-11} – 10^{-7} s. Therefore, a de-excitation process (fluorescence or phosphorescence) is more efficient and it will take place instead of internal conversion[18].

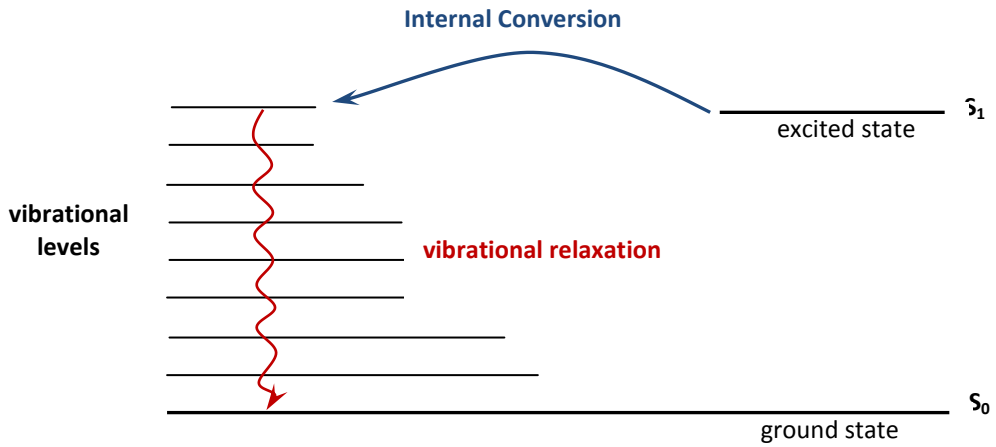

Figure 2.4. Internal conversion.

2.1.4 Fluorescence

Fluorescence is the emission of photons with the $S_1 \rightarrow S_0$ relaxation. It usually occurs after the internal conversion to lowest energy level of vibrational state of S_1. So its properties are independent on the excitation wavelength. Also, due to the energy loss during internal conversion and vibrational relaxation, the emission light carries less energy than the absorption light (see figure 2.5.). Therefore, compared with absorption spectra, the emission spectra shifts to longer wavelength (red region). The difference of wavelength between absorption and fluorescence is called Stokes shift.

It is worth mentioning that the emission of a photon is also a fast process (about 10^{-15} s), which is as fast as the absorption of a photon. But before the de-excitation process happens, the excited molecules have a lifetime of a few nanoseconds at S1 state[18].

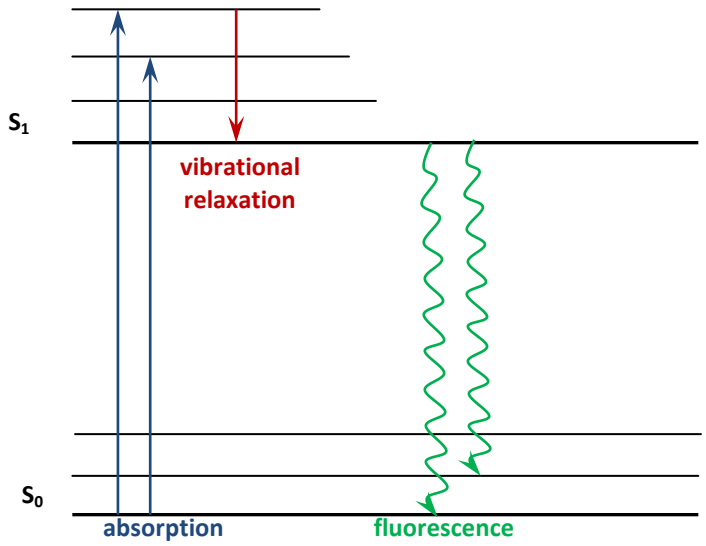

Figure 2.5. Fluorescence.

2.1.5 Intersystem crossing

Intersystem crossing is the de-excitation process from S_1 singlet state to T_1 triplet state (see figure 2.6.). It is spin-forbidden due to the change of spin multiplicity, but it is possible if spin-orbit coupling is strong enough (e.g. presence of heavy atoms). Once intersystem crossing

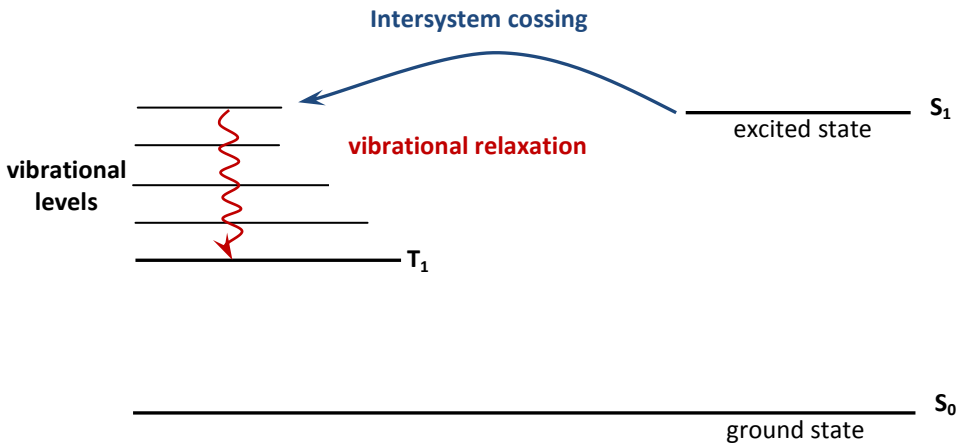

happens, the lifetime of T_1 can be as long as 10^{-6} s[18].

Figure 2.6. Intersystem crossing.

2.1.6 Phosphorescence

The de-excitation process of the emission of photons from T_1 to S_0 is called phosphorescence (see figure 2.7.). It is also forbidden, it only happens intersystem crossing and the presence of strong spin-orbit coupling. Other non-radiative processes can compete with phosphorescence, due to its low radiative rate constant (10^{-6} s). But at low temperatures and/ or in a rigid medium, phosphorescence is favored and is able to be observed.

The location of these de-excitation processes wavelengths depends on the difference of energy of the lowest vibrational state to the ground state. Since the lowest vibrational level of the singlet state is higher than that of triplet state, the fluorescence has lower wavelengths than phosphorescence[18].

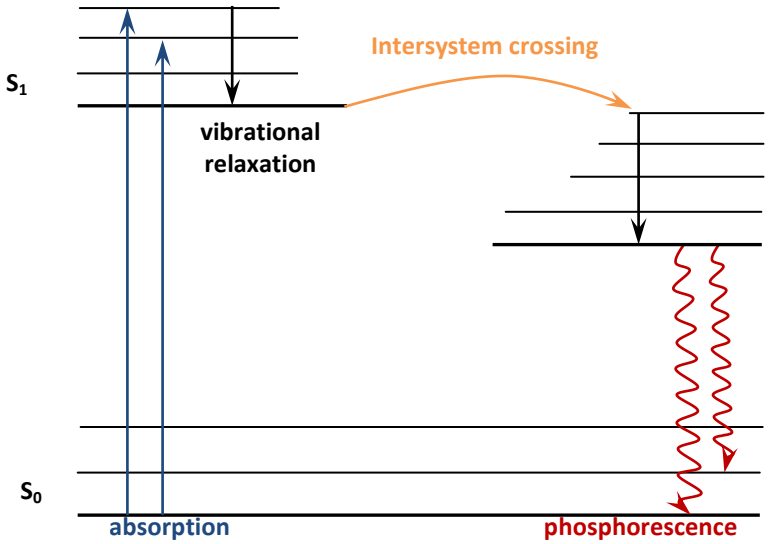

Figure 2.7. Phosphorescence.

2.1.7 Delayed fluorescence

When the energy difference between S1 and T1 is small, and the lifetime of T1 is long enough, the reverse process of intersystem crossing takes place. Since the energy level of lowest vibrational singlet state is still the same as before, it gives us same emission spectra, except a much longer decay time. This process is called delayed fluorescence (see figure 2.8.). Delayed fluorescence of E-type (first observed in eosin) is thermally activated. In another word, higher the

temperature is, more efficient it is. It is very common in fullerenes, but not in aromatic hydrocarbons, due to the relatively larger energy gap between S_1 and T_1[18].

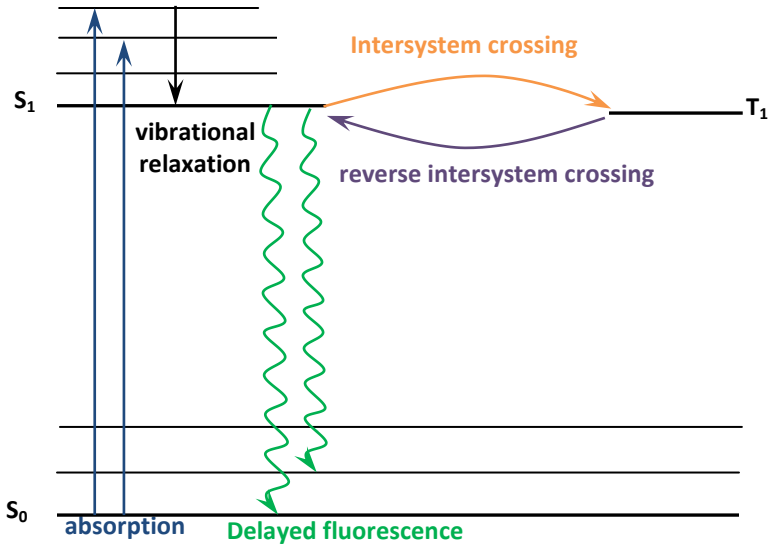

Figure 2.8. Delayed fluorescence.

2.1.8 Lifetimes

After a molecule being excited to the singlet state S_1, several deactivation processes can occur. It includes non-radiative de-excitation processes (internal conversion, intersystem crossing), and radiative de-excitation processes (fluorescence, phosphorescence, delayed fluorescence). These processes do not happen immediately and the molecule stays at the singlet state S_1 for certain time. The rate of de-excitation can be described by first order kinetics:

$$-\frac{d[A^*]}{dt} = k \cdot [A^*] \qquad \text{Eq. 2-2}$$

Where $[A^*]$ is the concentration of a species A in the excited state and k is the sum of all possible deactivation rates, which is further specified by:

$$k = \sum k_{deactivation} = k_{radiative} + k_{non-radiative}$$ Eq. 2-3

Integration of Eq . 2-2 gives:

$$[A^*] = [A^*] * e^{-kt}$$ Eq. 2-4

Also, the definition of the lifetime of excited state is $\tau = \frac{1}{k}$, so we have

$$[A^*]_t = [A^*]_0 \cdot e^{-\frac{t}{\tau}}$$ Eq. 2-5

This shows us that the fluorescence intensity decreases exponentially if the excitation does not exist. The fluorescence decay time τ defines the time window for various dynamic phenomena. It is usually in the range of $10^{-11} – 10^{-7}$ s for state S_1, while T_1 has a much longer lifetime from $10^{-6} – 10^{0}$ s[18].

2.1.9 Quantum yields

Quantum yield (Φ_F) is a critical parameter for sensor brightness, and it is defined by the ratio of amount of emitted photons and absorbed photons[18].

$$\Phi_F = \frac{k_{radiative}}{k_{radiative} + k_{non-radiative}} = k_r \tau$$ Eq. 2-6

The higher temperatures lead lower quantum yields, since non-radiative deactivation processes are more likely to take place.

2.1.10 Quenching

The discussion in previous sections talked about intrinsic de-excitation processes. Now we will discuss the intermolecular de-excitation phenomena, which has another molecule Q interacts with an excited molecule M^*. Quenching is the de-excitation process of the excited molecule M^* by the other molecule Q (quencher), with a rate constant k_q. Intermolecular processes which cause de-excitation can be the collision with heavy atoms, electron transfer, the formation of excimer / exciplex, proton transfer or energy transfer. The fluorescence characteristics (e.g. decay time, quantum yield) are affected by the quencher Q, since intrinsic and intermolecular de-excitation processes are competitors.

In our case, we only focus on the quenching through collisions. Collisions with heavy atoms or paramagnetic molecules (e.g. molecule oxygen) can deactivate an excited dye. The operating principle for oxygen sensor is the quenching of luminescence dye by molecule oxygen. During the quenching, oxygen molecules at triplet state get promoted to the singlet state and the dye transfers back to its ground state (as reaction below). This is a both lifetime shorten and quantum yield lower process.

$$A^* + {}^3O_2({}^3\Sigma) \rightarrow A + {}^1O_2({}^1\Delta)$$

Based on the relatively concentration of quencher, we divided quenching as static quenching and dynamic quenching. If the quencher is present at high concentration, it is more possible to find a quencher in reaction distance. When the probability is 1, the system shows simply diffusion-independent first order decay. In all other cases, this state is considered to be concentration-dependent static quenching. If the concentration of quencher is not high enough that nearly no

dye can be de-excited immediately, the diffusion of the excited dye or the quencher is necessary and it is rate-limited for the quenching. This is called dynamic quenching.

Oxygen dynamic quenching consists of two phases. First the quencher diffuses to the excited dye (and/ or the dye to the quencher when it is in solution). Second, the interaction between quencher and dye yields the de-excited luminophore. For this process, the first reaction is the rate-limited. Therefore, this process is a pseudo-first order reaction.

The Stern-Volmer relation (Eq. 2-7) gives us the idea of how fluorescence intensity (I) and lifetime (τ) changes in regarding of quenching (the concentration of quencher ([Q]), quenching rate constant (k_q)). The Stern-Volmer constant (K_{SV}) is the combination of non-quencher lifetime (τ_0) and quenching rate constant, which is an important parameter for sensor sensitivity[18].

$$\frac{I_0}{I} = \frac{\tau_0}{\tau} = 1 + k_q \cdot \tau_0 \cdot [Q] = 1 + K_{SV} \cdot [Q] \qquad \text{Eq. 2-7}$$

2.1.11 Excitation energy transfer/ FRET

It is important to be aware of the difference of radiative and non-radiative energy transfer. When the emission spectrum of the donor and the excitation spectrum are overlapped, some vibrational levels in the donor have identical energy as the corresponding energy level in the acceptor. This kind of excitation energy transfer is called non-radiative energy transfer or FRET, and it results from short- or long-range interactions between molecules, such as Coulombic and/ or intermolecular orbital overlap. In contrast, radiative energy transfer requires emission of photons at distances less than the wavelength. Basically, radiative transfer includes the emission of a

photon by a donor and the absorption of the photon by an acceptor. Usually we can observe a decrease of the donor fluorescence intensity in the region of spectral overlap[18].

2.1.12 Two-photon excitation

With the energy from the absorption of two photons, a molecule being promoted to an excited electronic state is called Two-photon excitation. It is a nonlinear process. Instead of one energetic photon absorbed, two less energetic photons are simultaneously absorbed to match the energy gap between ground and excited states. Quantum mechanically, the first photon excites the molecule to a virtual intermediate state, and followed by the second photon to bring it to the final excited state[19].

2.2 Optical sensor

Optical sensors, or opt(r)odes, are a group of chemical sensors in which utilizing electromagnetic radiation to generate analytical signals. The change of a specific parameter is used to interpret the interaction between the radiation and the sample[20]. Generally, an optical sensor consists of a chemical recognition unit (sensing element or receptor) and a transduction unit (transducer). The receptor produces the optical signal proportional to a certain parameter (e.g. the concentration of a given compound, pH, etc.). Then the transducer translates the optical sensor for processing[3, 21]. If the receptor is produced by synthesis, it is called "chemosensor". And "biosensor" defines sensors with a receptor consisting biological substance (e.g. enzymes, immunoglobulins, etc.)[22].

There are two main categories of optical sensors: intrinsic optical sensor and extrinsic optical sensor. An intrinsic optical sensor is only responding to the certain parameter of the analyte. An

extrinsic optical sensor produces optical signals corresponding to the interaction of the analyte and the indicator, while the analyte itself doesn't generate any signals.

Optical sensors have been used widely in different fields, including biomedical research[23], marine biology[24], biological and toxicological screening[25, 26], and food packing[27], for measurements of oxygen, CO_2, NH_3, pH and other ionic species.

2.2.1 Design of an optical sensor

Normally, an optical sensor at least consists of two units: an optical detection system and immobilization system. The detection system can be direct sensing or indicator-mediated sensing. For directing sensing, the analyte can be measured directly by some intrinsic optical property (e.g. absorption, luminescence). While the indicator-mediated sensing system, the analyte concentration or other properties is monitored by an intermediate agent, usually an analyte-sensitive dye (indicator), to present as optical change[9, 28].

Immobilization of the indicator also plays important role in the design of optical sensor. There are three approach used widely.

Impregnation – apply physical absorption, chemisorption or electrostatic bonding to immobilize the indicator to the polymer matrix[3].

Covalent bonding – the indicator is covalently bonded to the polymer matrix[29, 30].

Doping – the indicator is entrapped in the matrix during the polymerization process, where the indicator is simply mixed to the polymer stock solution[30].

2.2.2 Optical Oxygen sensor

Among various optical sensors, oxygen sensors are widely used and well developed. The principle of optical oxygen sensors is dynamic quenching of the luminescence of indicator by molecule oxygen, which shortens the lifetime of the indicator. The triplet state is oxygen's ground state. Typically, the indicator is immobilized in an oxygen permeable polymer matrix[5].

This polymeric matrix acts as solvent for the indicator and helps it remain same concentration. Also, this matrix protects the indicator from ions or other species. The sensitivity of the sensor depends on the gas permeability of the matrix, and indicator decaytime. The permeability of oxygen to the matrix depends on diffusion constant and the solubility coefficient. Commonly used materials for matrix are organic glassy polymers (e.g. polystyrene, poly(methylmethacrylate), fluorinated polymers, cellulose derivatives) and inorganic polymers (e.g. silicones and sol gels)[31]. Some materials permeability coefficients are listed in table 2.2.

Table 2.2. Permeability rates of commonly used sensor matrices[5]

Polymer matrix	**Permeation rate for oxygen [$cm^2s^{-1}mmHg^{-1}$]**
Poly(methylmethacrylate)	9
Polystyrene	2.63
Polyvinylchloride	0.34
Poly(2,2,2-trifluoroethylmethacrylate)	32
Ethylcellulose	11.0
Cellulose acetate	5.85
Poly(dimethylsiloxane)	695

The relation of indicator lifetime and oxygen concentration can be described in Stern-Volmer-Plot (see Eq. 2-7). However, this is for the ideal case when the indicator distributes evenly on the matrix and has same accessibility to be quenched by molecule oxygen.

The immobilization of the indicator to the matrix is heterogenic, and it is more suitable for the Two-Site-Model, which assumes two different quenching domains (see Eq. 2-8)[32].

$$\frac{I_0}{I} = \frac{1}{\frac{f}{1 + K_{SV_1} \cdot [O_2]} + \frac{1 - f}{1 + K_{SV_2} \cdot [O_2]}} \qquad \text{Eq. 2-8}$$

To simplify this model, assume that quenching is only possible in one of the two domains.

This is a rather unrealistic assumption but reduces the fit parameters to two and still fits well for many practical applications (see Eq. 2-9).

$$\frac{I_0}{I} = \frac{1}{\frac{f}{1 + K_{SV_1} \cdot [O_2]} + \frac{1 - f}{1}} \qquad \text{Eq. 2-9}$$

2.2.3 Indicators for optical oxygen sensors

The selection of optical oxygen sensors indicator dyes depend on the area of application, consequently, the matrix material and detection method. For example, applications of measuring oxygen in live cells and in tissues, it is necessary to consider the autofluorescence generated by biological substances, like proteins, DNA, and melanin. To minimize the absorption and scattering of the excitation and emission light in the tissue, it is more likely to emply indicators have longwave-shifted absorption (590 – 650 nm) and emission (730 – 900 nm) bands[33, 34].

There are two main groups of optical oxygen sensors: absorption- and luminescence-based indicators. To date, luminescence-based indicators are most widely used in different fields of science. Also luminescent indicators can be classified into several groups: polycyclic aromatic hydrocarbons, polypyridyl complexes, metal porphyrins, syslometallated complexes, and complexes with rarely used central atoms. Among them, Pt(II) and Pd(II) are the most common used luminophores, due to their properties of strong phosphorescence at room temperature, moderate to high molar absorption coefficients, large Stokes' shifs, relatively long phosphorescence lifetime, variation in spectral properties, possibility of synthetic modification to introduce the required functionalities. Many researchers have been working on Pt(II) and Pd(II) pophyrin complexes to improve the photophysical properties to make it more suitable for oxygen sensing in different areas and conditions[10].

2.2.4 Conjugated polymers

Conjugated polymers are organic macromolecules which consist at lease of one backbone chain of alternating double- and single-bonds. The interest increased in conjugated polymers due to the substantial π-clectron delocalization along their backbones, which gives them optical[35] and nonlinear optical properties[36-38]. These properties make conjugated polymers become practical for applications in information storage, optical signal processing, substitution for batteries, and solar energy conversion materials[39].

Furthermore, electroluminescence from conjugated polymers makes it even more popular for a rapid expanding application areas[40, 41]. This luminescence efficiency is related to the delocalization and polarization of the electronic structure. It is a main advantage of conjugated polymers used as sensor materials over other materials that the potential of the conjugated

polymers to exhibit collective properties that are sensitive to very small minor perturbations[42]. For example, some work has been done to integrated conjugated polymers and porphyrins in one system as oxygen sensor[16, 43].

2.2.5 Oxygen-sensitive nanoparticles

Oxygen sensors can be realized in different forms, like planar optodes, fiber sensor, sensor paints, microsensor. Nanoparticle-based oxygen attracts more attention for its higher signals at lower oxygen levels[15], which is suitable for low concentration oxygen measurement for imaging and dynamic monitoring in intracellular or extracellular environments. Also due to its small size, inert matrix, biocompatibility, another advantage is they are physically disruptive to the surroundings[44], which can be applied for non-invasive real-time measurements[11, 12, 45].

3 Methods

3.1 Photophysical Measurements

3.1.1 Absorption

Absorption measurements were performed between 800nm and 350nm on a "Varian Cary 50 Conc "UV-Vis spectrophotometer by Varian, Palo Alto, United States (www.varianinc.com), set at a fast scan rate using baseline correction and an adequate blank sample. Hellma 100-QS 10mm precision cuvettes or Hellma 101-OS 10mm precision cuvettes were used. Molar absorption coefficients were calculated using Lambert-Beers law.

3.1.2 Emission and Excitation Spectra

Emission and excitation spectra were recorded on a Hitachi-F-7000 spectrofluorometer in Hellma 101-OS 10mm precision cuvettes or Hellma screw-cap fluorescence cuvettes and corrected for detector response.

3.1.3 Single Photon Counting

The fluorescence decay times were acquired using single photon counting technique on a FluoroLog Spectrofluorometer from Horiba Scientific equipped with a DeltaHub module. Data were fitted using a mono-exponential fit or bi-exponential fit.

3.2 Structural and Chemical Measurements

3.2.1 NMR

^{1}H NMR spectra were recorded on a 300MHz Bruker instrument (www.bruker.com). The analysis of the data was conducted with MNova NMR software (www.mestrelab.com).

3.2.2 Size and Zeta-potential

The size of the beads and Zeta potential were determined with a particle size analyzer Zetasizer Nano ZS (www.malvern.de).

4 Experimental

4.1 Materials

All the used chemicals are listed in Table 4.1.

Table 4.1. Used chemicals.

Chemical	Supplier	CAS number
Acetone	Brenntag	76-64-1
Dichloromethane	VWR	75-09-2
Dichloromethan anhydrous	Sigma-Aldrich	75-09-2
N,N-Dimethylformamid anhydrous	Sigma-Aldrich	68-12-2
Ethylacetate	VWR	141-78-6
Ethanol	Brenntag	64-17-5
Tetrahydrofuran	VWR	109-99-9
Toluene	VWR	108-88-3
1,2,4-Trimethylbenzene	Sigma-Aldrich	95-63-6
Silica Gel	Acros	112926-00-8
Tetrakis(triphenylphosphin)palladium	ABCR	14221-01-3
K_2CO_3	Roth	584-08-7
Methanol	Roth	67-56-1
Sodium hydroxide (0.1 M)	Roth	1310-73-2
Sodium sulphate	VWR	7757-82-6
Sodium chloride	Fluka	7647-14-5
9,9-Diheptylfluorene-2,7-diboronic acid	Frontier	916336-19-1
4-(tert-Butyl)phenylboronic acid	Frontier	123324-71-0
[9,9-Di(p -tolyl)-fluoren-2,7-diyl]diboronic acid	Lumtec	
2,7-Dibromo-9,9-di-p -tolyl-9H -fluorene	Lumtec	357645-37-5
4,7-Bis(5-bromothiophen-2-yl) benzo[c][1,2,5]thiadiazole	Lumtec	288071-87-4

3,3'-(2,7-Dibromo-9H-fluorene-9,9-diyl)bis(N,N-dimethylpropan-1-amine)	Lumtec	673474-73-2
4,7-Dibromobenzo[c]-1,2,5-thiadiazole	Sigma-Aldrich	15155-41-6
Bis(di-tert-butyl(4-dimethylaminophenyl)phosphine)dichloropalladium(II)	Acros	887919-35-9
1,5-Diiodopentane	ABS	628-77-3
1-Bromo-2-(2-methoxyethoxy)ethane	ABS	54149-17-6
Tetrabutylammonium bromide	Sigma-Aldrich	1643-19-2
2,7-Dibromofluorene	Sigma-Aldrich	16433-88-8
$H_2TPTBPtBu_4Br_4$	synthesized at TU Graz	
Pt(II)–5,15-di(pentafluorophenyl)-10,20-di(4-bromophenyl)porphyrin (PtTFPP)	synthesized at TU Graz	

4.2 Monomer synthesis

4.2.1 Anionic monomer – Dimethyl 3,3'-(2,7-dibromo-9H-fluorene-9,9-diyl)dipropanoate [46]

2,7-Dibromofluorene (500 mg, 1.55 mmol), methyl acrylate (430.5 mg, 5 mmol) tetrabutylammonium bromide (50 mg, 0.15 mmol) and toluene (2.5 ml) were added to a small round bottom flask with a Teflon-coated stirbar. Next 1 ml of 50% NaOH (aq) was added while stirring. The reaction was allowed to proceed overnight at room temperature. The next day the toluene layer was transferred to a flask and the aqueous layer was extracted with two portions of toluene. The organic layers are combined, dried with Mg_2SO_4, and filtered. Silica (2 g) was added to the filtrate and the solution was evaporated under N_2. The product was purified via column chromatography on silica gel packed with cyclohexane. Impurities were washed out by toluene and the clean product was eluted with a mixture of toluene and ethyl acetate (1:1). After drying in vacuum oven overnight, the pure product was obtained as a white solid. Yield 2.09 g. ^{1}H NMR (300 MHz, $CDCl_3$) δ, ppm: 7.55-7.46, m, 6H, Ar; 3.49, s, 6H, -$COOCH_3$; 2.37, t, 4H, CH_2-$\underline{CH_2}$-$COOCH_3$; 1.57, t, 4H, $\underline{CH_2}$-CH_2-$COOCH_3$. Figure 4.1 Shows ^{1}H and COSY NMR spectra of the compound.

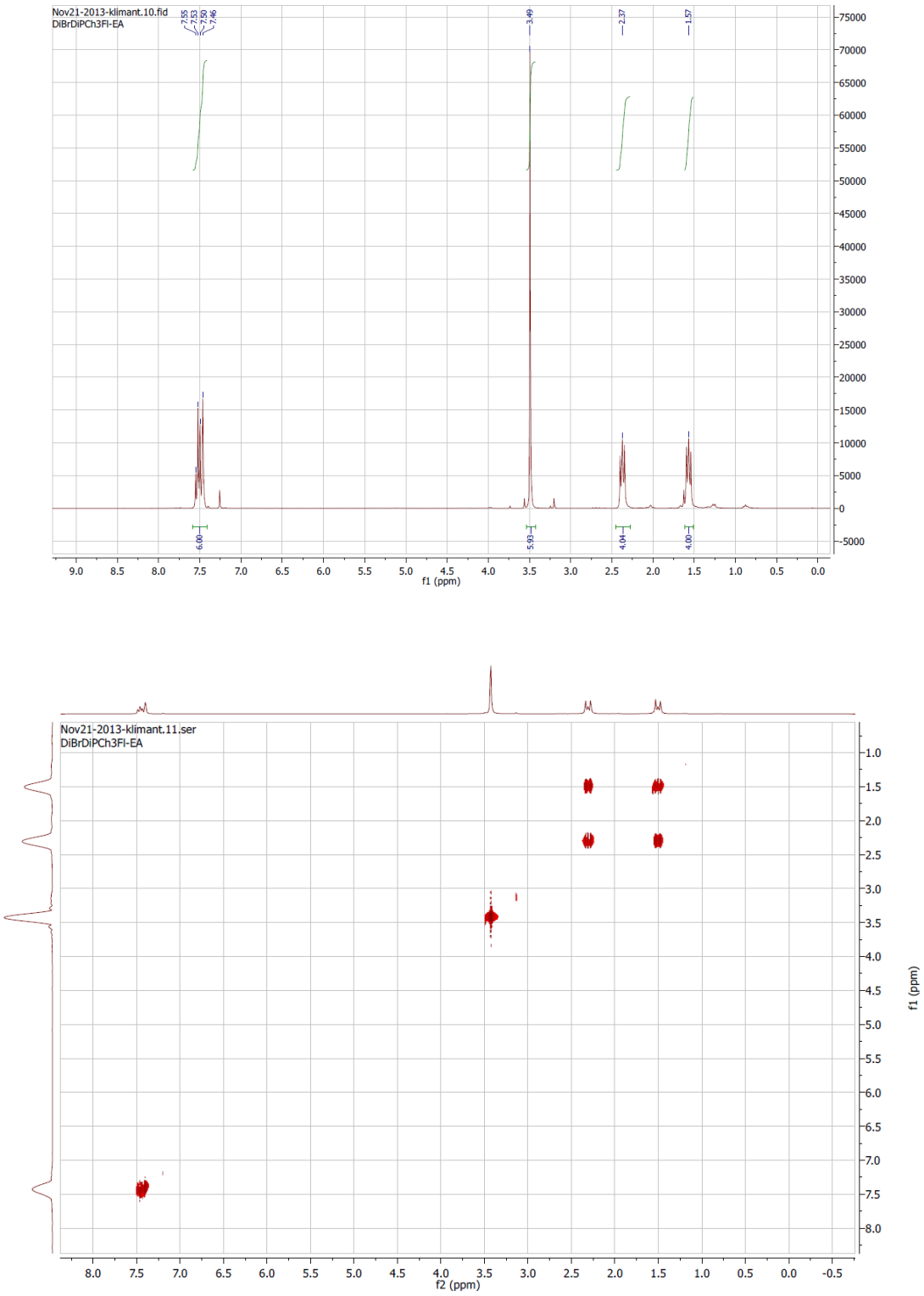

Figure 4.1. ^{1}H and COSY NMR spectra of the dimethyl 3,3'-(2,7-dibromo-9H-fluorene-9,9-diyl)dipropanoate.

4.3 Dye synthesis

4.3.1 PtTPPtBuBP

Platinum (II) meso-tetra(4-bromophenyl)tetra(*tert-butyl*)benzoporphyrin

$H_2TPTBPtBu_4Br_4$ (500 mg, 0.369 mmol) was dissolved in 250 ml trimethylebenzene and heated to 155 ℃ in a 2-neck round bottle. N_2 was bubbled through the reaction mixture and $Pt(BN)_2Cl_2$ (260 mg, 0.554 mmol) was added in small pre-dissolved portions over 4 hours. The reaction was monitored via UV-Vis spectroscopy. The solvent was removed using a rotary evaporator at 70 ℃ and the crude product was purified using column chromatography (Al_2O_3, Cyclohexene/Dichloromethane 5/1). The solvent was removed and the product was placed in a 2-neck round-bottle with cold finger. The viscous product was heated to 350 ℃ under high vacuum to remove side products (Yield 404 mg, 0.263 mmol, 71%).

4.4 Conjugated polymers synthesis

The conjugated polymers were prepared through Suzuki coupling between various platinum (Ⅱ) porphyrin complexes and one to one ratio of diboronic acid and dibromo derivatives as building blocks. Different dibromo derivatives were used to give different functions to the conjugated polymers. For example, 4,7-bis(5-bromothiophen-2-yl)benzo[c][1,2,5]thiadiazoles shifts the excitation and emission wavelength of conjugated polymers to near-infrared(NIR) wavelength.

4.4.1 PtTFPP integrated cationic conjugated polymer

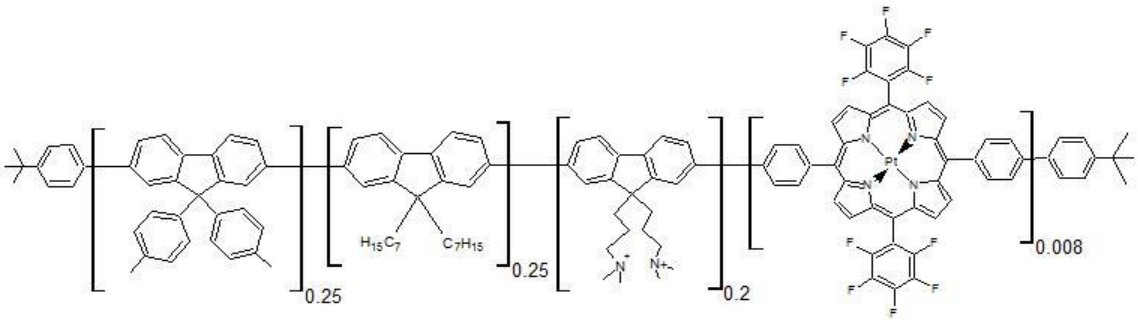

Figure 4.2. Structure of PtTFPP integrated cationic conjugated polymer

[9,9-di-p-tolyl-fluoren-2,7-diyl]diboronic acid (110.7 mg, 0.25 mmol), 9,9-diheptylfluorene-2,7-diboronic acid (114.8 mg, 0.25 mmol), 2,7-dibromo-9,9-di-p-tolyl-9H-fluorene (154.4 mg, 0.3 mmol), 3,3'-(2,7-dibromo-9H-fluorene-9,9-diyl)bis(N,N-dimethylpropan-1-amine) (100.9 mg, 0.2 mmol), and Pt(II)–5,15-di(pentafluorophenyl)-10,20-di(4-bromophenyl)porphyrin (PtTFPP) (9 mg, mmmol) were dissolved in the mixture of 5 ml toluene and 1.7 ml tetrahydrofuran in Schlenk flask with a Teflon-coated stir bar. Next, potassium carbonate (276 mg, 2 mmol) dissolved in 1.5 ml deionized (DI) water and bis(di-tert-butyl(4-dimethylaminophenyl)phosphine)dichloropalladium(II) (10.4mg, 3mol%) dissolved in 1 ml toluene were added into Schlenk flask while stirring. The reaction was allowed to proceed overnight at 80 °C. The next day, 2,7-dibromo-9,9-di-p-tolyl-9H-fluorene (10.3 mg, 0.02 mmol) and 4-tert-butylphenylboronic acid (8.9 mg, 0.05mmol) were added into reaction with 1.5 hours in between. After another 1.5 hour the flask was left at room temperature to cool down. The organic layer was transferred to a flask and the aqueous layer was extracted with two portions of dichloromethane. The organic layers are combined, dried with Mg_2SO_4, and filtered, if necessary. Then organic phase was added dropwise into 6 times volume of methanol to precipitate the

product. After filtering, the sediments were dried on filter paper in oven at 60 °C overnight. The polymer was obtained as a red solid (225.3 mg, 66.0% yield).

The polymer was rendered cationic via alkylation. 50 mg of the polymer, 2.5 ml of toluene, 24.2 mg (0.2 mmol) of potassium carbonate and 14mg (0.1 mmol) of methyl iodide were added into Schlenk flask with a Teflon-coated stirbar. The reaction was done at 80 °C under argon gas for 4 hours. The organic layer was transferred to a flask. After distillation at reduced pressure, the PtTFPP integrated cationic conjugated polymer was dissolved in acetone and THF mixture as "cocktail" to make particles.

4.4.2 PtTFPP integrated anionic conjugated polymer

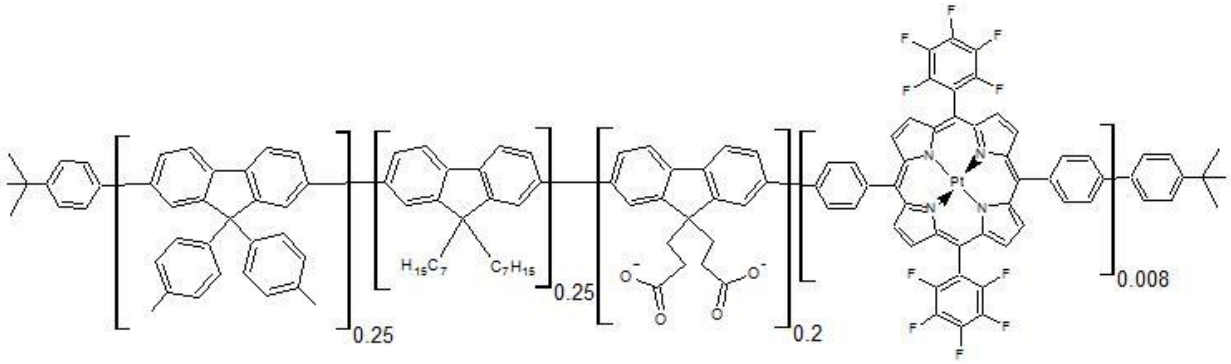

Figure 4.3. Structure of PtTFPP integrated anionic conjugated polymer

[9,9-di-p-tolyl-fluoren-2,7-diyl]diboronic acid (110.7 mg, 0.25 mmol), 9,9-diheptylfluorene-2,7-diboronic acid (114.8 mg, 0.25 mmol), 2,7-dibromo-9,9-di-p-tolyl-9H-fluorene (154.4 mg, 0.3 mmol), dimethyl 3,3'-(2,7-dibromo-9H-fluorene-9,9-diyl)dipropanoate (101.3 mg, 0.2 mmol), and PtTFPP (9 mg) were dissolved in 5 ml toluene and 1.7 ml tetrahydrofuran (THF) mixture in Schlenk flask with a Teflon-coated stir bar. Next, potassium carbonate (276 mg, 2 mmol) dissolved in 1.5 ml deionized (DI) water and bis(di-tert-butyl(4-

dimethylaminophenyl)phosphine)dichloropalladium(II) (10.4mg, 3mol%) dissolved in 1 ml toluene were added into Schlenk flask while stirring. The reaction was allowed to proceed over night at 80 °C. The next day, 2,7-dibromo-9,9-di-p-tolyl-9H-fluorene (10.3 mg, 0.02 mmol) and 4-tert-butylphenylboronic acid (8.9 mg, 0.05mmol) were added into reaction with 1.5 hours in between. After another 1.5 hour, the reaction was done and left at room temperature to cool down. The organic layer was transferred to a flask and the aqueous layer was extracted with two portions of dichloromethane. The organic layers are combined, dried with Mg_2SO_4, and filtered, if necessary. Then organic phase was added dropwise into 6 times volume of methanol to precipitate the product. After filtering, the sediments were dried on filter paper in oven at 60 °C overnight. The polymer was obtained as a red solid (237.2 mg, 85.4% yield).

The polymer was rendered anionic via hydrolysis. 50 mg of the polymer, 5 ml of THF, and 100 µl of 1M NaOH were added into a flask with a Teflon-coated stir bar. The reaction was done at 40 °C for 1 hour. The PtTFPP integrated anionic conjugated polymer was dissolved in additional 7.5 ml THF and 12.5 ml acetone solution as "cocktail" to make particles.

4.4.3 PtTFPP integrated "zwitterionic" conjugated polymer

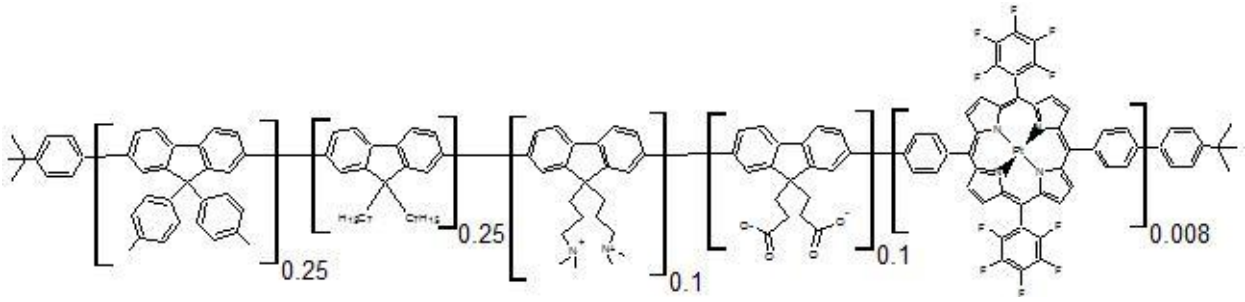

Figure 4.4. Structure of PtTFPP integrated zwittertionic conjugated polymer

The basic procedure of Suzuki coupling is similar as PtTFPP integrated cationic/ anionic conjugated polymers, except we have both cationic and anionic monomers inside. The following components were used: [9,9-di-p-tolyl-fluoren-2,7-diyl]diboronic acid (110.7 mg, 0.25 mmol), 9,9-Diheptylfluorene-2,7-diboronic acid (114.8 mg, 0.25 mmol), 2,7-dibromo-9,9-di-p-tolyl-9H-fluorene (154.4 mg, 0.3 mmol), 3,3'-(2,7-dibromo-9H-fluorene-9,9-diyl)bis(N,N-dimethylpropan-1-amine) (100.9 mg, 0.2 mmol), dimethyl 3,3'-(2,7-dibromo-9H-fluorene-9,9-diyl)dipropanoate (101.3 mg, 0.2 mmol), and PtTFPP (9 mg).

To have both cationic and anionic monomers to be functionalized, both alkylation and hydrolysis have been done, in the same order. The "cocktail" of the polymers in 25 ml THF and acetone mixture was obtained to make particles.

4.4.4 PtTPTtBuBP integrated cationic conjugated polymer

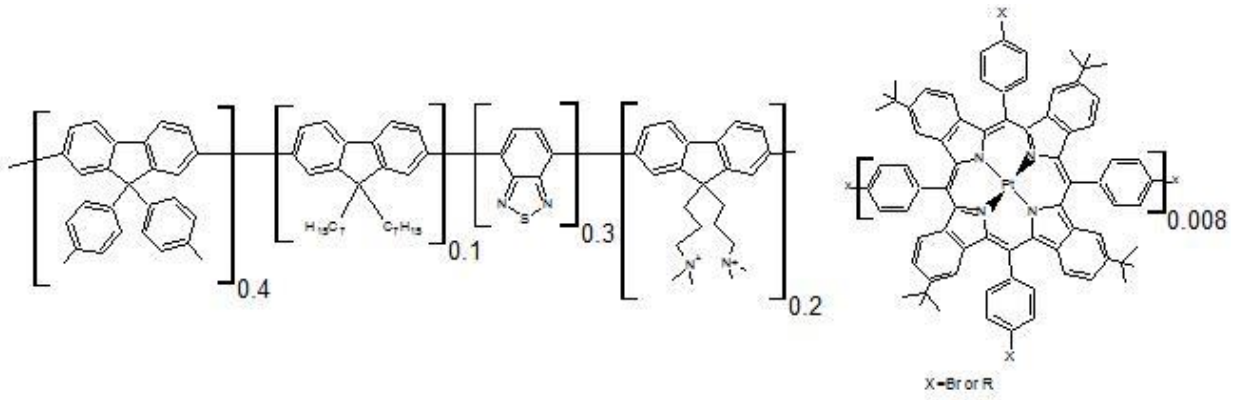

Figure 4.5. Structure of PtTPTtBuBP integrated cationic conjugated polymer

[9,9-di-p-tolyl-fluoren-2,7-diyl]diboronic acid (177.2 mg, 0.4 mmol), 9,9-diheptylfluorene-2,7-diboronic acid (45.9 mg, 0.1 mmol), 4,7-dibromobenzo[c]-1,2,5-thiadiazole (89.9 mg, 0.3mmol),

3,3'-(2,7-dibromo-9H-fluorene-9,9-diyl)bis(N,N-dimethylpropan-1-amine) (100.9 mg, 0.2mmol), and PtTPTBTPF (7 mg) were dissolved in 5 ml toluene and 1.7 ml THF mixture in Schlenk flask with a Teflon-coated stir bar. Next, potassium carbonate (276 mg, 2 mmol) dissolved in 1.5 ml deionized (DI) water and bis(di-tert-butyl(4 dimethylaminophenyl)phosphine)dichloropalladium(II) (10.4mg, 3mol%) dissolved in 1 ml toluene were added into Schlenk flask while stirring. The reaction was allowed to proceed overnight at 80 °C. The next day, 4,7-dibromobenzo[c]-1,2,5-thiadiazole (5.99 mg, 0.02 mmol) and 4-tert-butylphenylboronic acid (8.9 mg, 0.05mmol) were added into reaction with 1.5 hours in between. After another 1.5 hour, the reaction was done and left at room temperature to cool down. The following procedures are same as PtTFPP-integrated cationic conjugated polymers. A green solid was obtained as product. (114.0 mg, 53.8% yield).

To render the polymer cationic, the alkylation was performed using the procedure established for PtTFPP-modified polymers

4.4.5 PtTPTtBuBP integrated anionic conjugated polymer

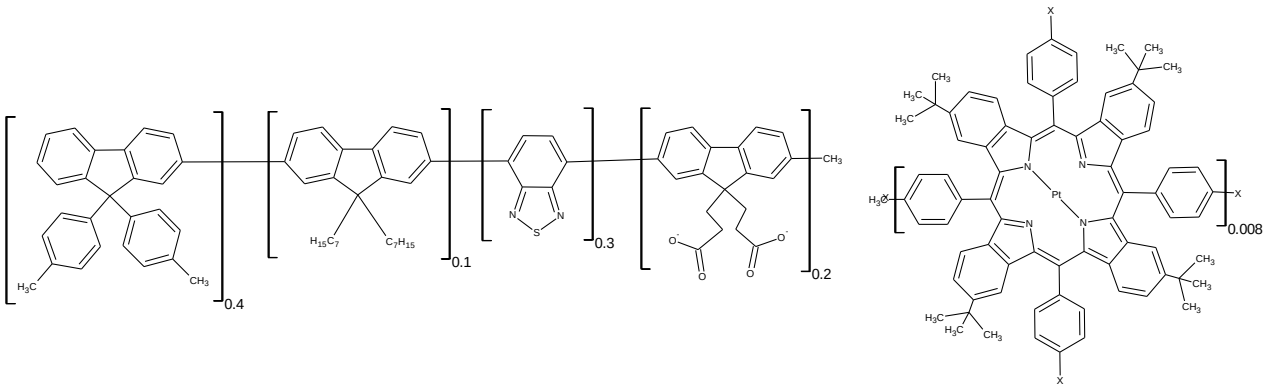

Figure 4.6. Structure of PtTPTtBuBP integrated anionic conjugated polymer

[9,9-di-p-tolyl-fluoren-2,7-diyl]diboronic acid (177.2 mg, 0.4 mmol), 9,9-diheptylfluorene-2,7-diboronic acid (45.9 mg, 0.1 mmol), 4,7-dibromobenzo[c]-1,2,5-thiadiazole (89.9 mg, 0.3mmol), dimethyl 3,3'-(2,7-dibromo-9H-fluorene-9,9-diyl)dipropanoate (101.3 mg, 0.2 mmol), and PtTPTtBuBP (3.5 mg) were dissolved in 5 ml toluene and 1.7 ml THF mixture in Schlenk flask with a Teflon-coated stir bar. Next, potassium carbonate (276 mg, 2 mmol) dissolved in 1.5 ml deionized (DI) water and Bis(di-tert-butyl(4-dimethylaminophenyl)phosphine)dichloropalladium(II) (10.4mg, 3mol%) dissolved in 1 ml toluene were added into Schlenk flask while stirring. The reaction was allowed to proceed over night at 80 °C. The next day, 4,7-Dibromobenzo[c]-1,2,5-thiadiazole (5.99 mg, 0.02 mmol) and 4-tert-Butylphenylboronic acid (8.9 mg, 0.05mmol) were added into reaction with 1.5 hours in between. After another 1.5 hour, the reaction was done and left at room temperature to cool down. The procedure used for the PtTFPP-integrated anionic conjugated polymers was used. A green solid was obtained as product. (86.0 mg, 42.0 % yield).

To have the anionic function, hydrolysis was done the next day, which is exactly the same as alkylation for PtTFPP integrated anionic conjugated polymers.

4.5 Preparation of conjugated polymer-based nanoparticles

First, 50 mg of the conjugated polymer were dissolved in 30 ml of acetone : THF mixture. The solution was transfered into 150 ml glass beaker equipped with a teflon-coated stir bar.. Then, 125 ml of DI water was added to the stirred solution (400 rpm) within 3 seconds. A transparent colored dispersion of the nanoparticles was formed. The dispersion of the nanoparticles was placed in 250 ml round flask and acetone and THF and partly water were removed reduced

pressure (by gradually reducing pressure up to about 80 mbar). The dispersion was concentrated to about 35 ml and was stored in screw cap vials at 4 ℃.

5 Results and discussion

The aim of this work is the development of conjugated polymer-based oxygen sensitive nanoparticles, with high brightness, under dual emission for ratiometric measurements, functional groups for water dispersibility and cell penetration.

The scientific strategy to obtain this kind of oxygen sensitive nanoparticles was to co-polymerize oxygen indicator, additional functional groups, e.g. the charged group, inside of the conjugated polymers.

5.1 Synthetic considerations

Suzuki coupling is an established way to produce conjugated polymers. It is modular, different blocks (dibromo- and diboronic acid derivatives) can be combined in an alternating polymer. Functionalities can be incorporated. Better use neutral functionalities and render them charged already in the polymer. Neutral polymer is easier to obtain, no redistribution of the monomers between organic and aqueous phases, easier purification of the uncharged polymer from oligomers. Other dyes can be incorporated as well (such as porphyrins used here). Dibromo derivatives are preferable; however 4 Br derivatives (see Pt-bennzoporphyrins) may be used in small concentration (which is high enough for the applications). The risk of cross-linking is small at these concentrations.

5.2 Brightness of conjugated polymer-based oxygen-sensitive nanoparticles

5.2.1 PtTFPP integrated conjugated polymer-based oxygen-sensitive nanoparticles

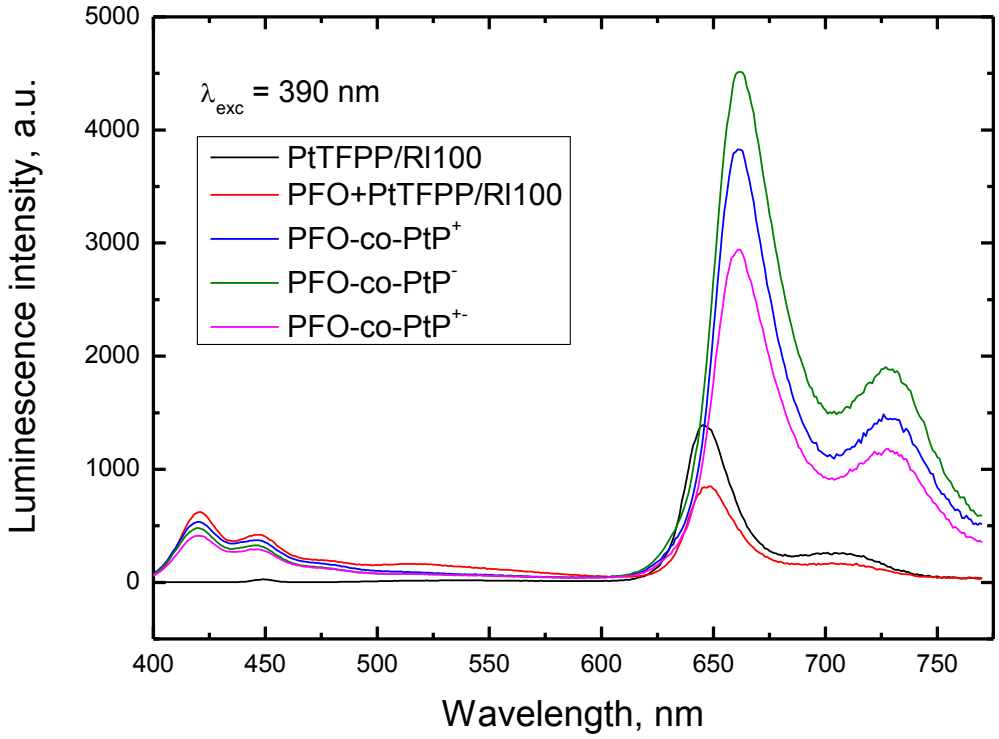

Figure 5.1. Corrected Emission spectra of PtTFPP integrated conjugated polymer-based oxygen sensitive nanoparticles (λ_{exc} = 390 nm, identical absorption of all samples at this wavelength)

The brightness of three kinds of PtTFPP integrated conjugated polymer-based oxygen-sensitive nanoparticles we prepared has been compared with two other kinds of oxygen-sensitive nanoparticles we worked on before. PtTFPP-RL-100 nanoparticles have 1.5% w/w dye incorporated in highly positively charged Eudragit RL-100 polymer by means of physical

inclusion[12]. Another oxygen nanosensor PFO-PtTFPP-RL-100 has the hydrophobic conjugated polyfluorene PFO (acting an energy donor) incorporated along with the oxygen indicator PtTFPP (acting as an energy acceptor) in RL-100[16]. It also allows for ratiometric or multiphoton imaging of oxygen. Both of these kinds of oxygen sensitive nanosensors show good brightness.

Comparing emission spectra of these oxygen nanosensors with 390 nm wavelength excitation, a significant improvement of brightness has been achieved by the synthesis of PtTFPP integrated conjugated polymer-based oxygen sensitive nanoparticles. Brightness of the.cationic, anionic and zwitterionic polymeric particles is similar. It is around 6 times and 4 times brighter than PtTFPP-RL-100 and PFO-PtTFPP-RL-100 nanoparticles, respectively. Similarly to the PFO-PtTFPP-RL-100 particles, the new polymeric beads allow for ratiometric measurement of oxygen due to the emission in both blue and red part of the spectrum.

It is interesting to note that the emission wavelength of PtTFPP in conjugated polymer-based nanoparticles is slightly shifted (about 15 nm) to longer wavelength. This is likely to be caused by increased pi-conjugation of the porphyrin incorporated into the conjugated polymer.

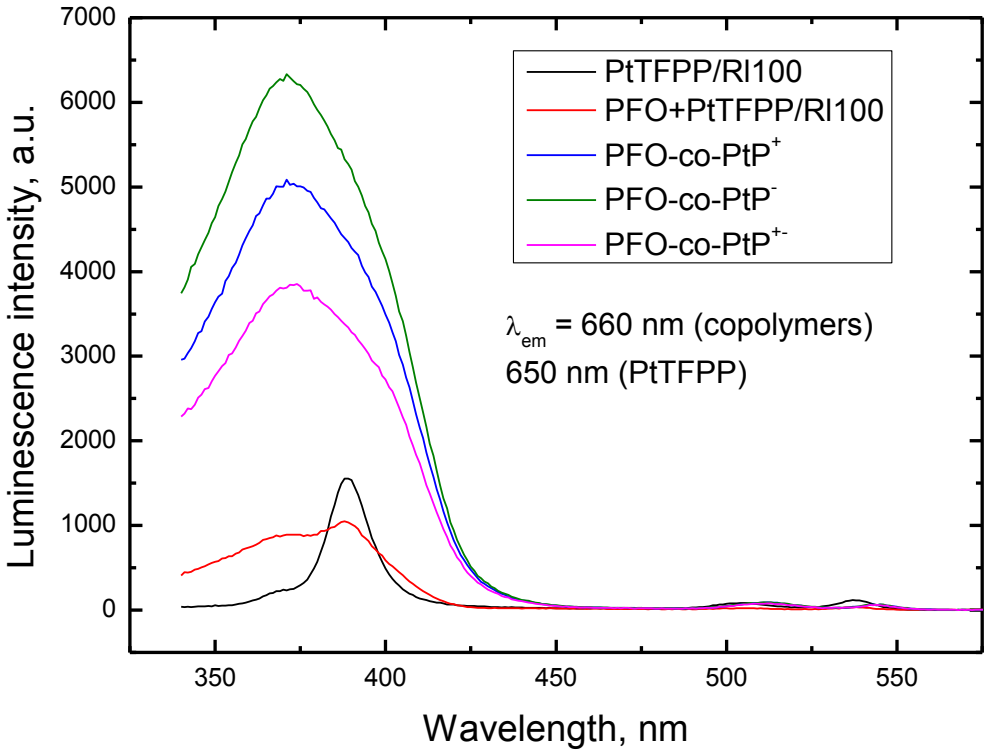

Figure 5.2. Excitation spectra of PtTFPP integrated conjugated polymer-based oxygen sensitive nanoparticles. (λ_{em} = 660 nm, conjugated polymers; λ_{em} = 650 nm PtTFPP)

Excitation spectra of PtTFPP integrated conjugated polymer-based oxygen sensitive nanoparticles indicates that the energy transfer from conjugated polymers to oxygen indicator (PtTFPP) is very efficient. Indeed, the excitation arises from the conjugated polymer, and only very small bans corresponding to the direct excitation of PtTFPP (510 and 540 nm) are visible.

We also noticed that, at the maxima emission wavelength of PtTFPP (650 nm in RL-100 polymer matrix, 660 nm in conjugated polymer matrix), excitation via conjugated polymer in conjugated polymer matrix is 5 – 6 times higher than in RL-100 polymer matrix . So we are able

to say the energy transfer in conjugated polymer is significantly efficient in our conjugated polymer-based oxygen sensitive nanoparticles.

5.2.2 PtTPTtBuBP integrated conjugated polymer-based oxygen-sensitive nanoparticles

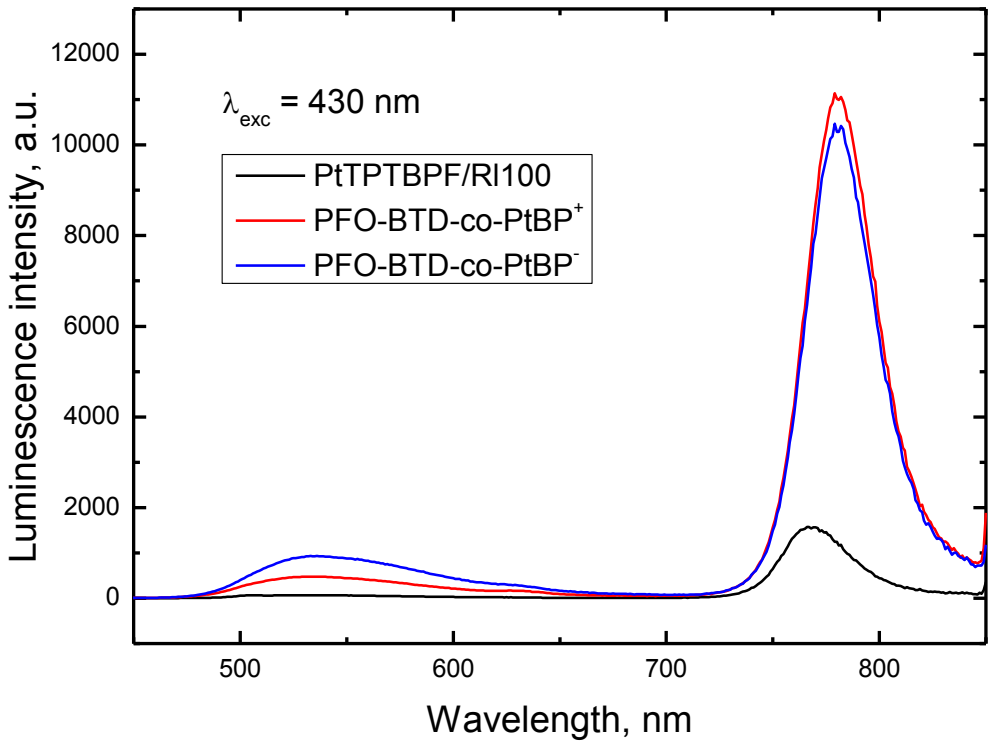

Figure 5.3. Corrected Emission spectra of PtTPTtBuBP integrated conjugated polymer-based oxygen sensitive nanoparticles (PFO-BTD-co-PtBP) and PtTPTBPF-doped Rl-100 nanoparticles used for comparison (λ_{exc} = 430 nm, the absorption at this wavelength is kept constant for all the materials))

Two kinds of PtTPTtBuBP integrated conjugated polymer-based sensitive nanoparticles have been prepared. One is positively charged and the other is negatively charged. Compared toPtTPTBPF incorporated RL-100 nanosensor, a factor of 6 of brightness enhancement has been achieved by conjugated polymer-based nanosensor. Importantly, the green emission originating from the conjugated polymer can again be used for the ratiometric referencing.

The maxima emission wavelength of PtTPTBPF is around 780 nm. This near-infrared emission spectra is more preferred, since it reduced the noise of autofluorescence in biological system. Again, conjugation may slightly affect the emission of the porphyrin in the conjugated polymer (a bathochromic shift of 10 nm compared to the PtTPTBPF-based particles). However, the electron-donating t-Bu groups of the porphyrin may also be responsible for this effect.

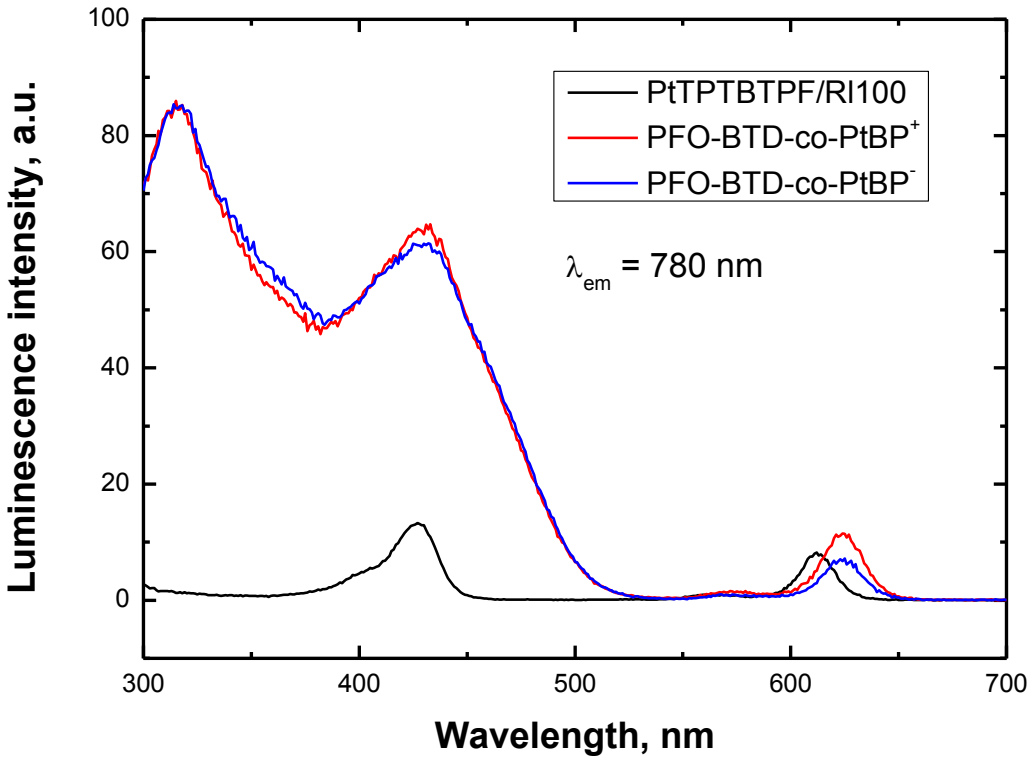

Figure 5.4. Excitation spectra of PtTPTtBuBP integrated conjugated polymer-based oxygen-sensitive nanoparticles and PtTPTBPF-doped Rl-100 nanoparticles used as a reference. (λ_{em} = 780 nm)

An efficient energy transfer from the conjugated polymer to PtTPTtBuBP in conjugated polymer-based nanoparticles is evident (Figure 5.4.). Corresponding to the emission spectra, enhancement by the factor of 6 or more is established in both cationic and anionic conjugated polymer-based oxygen sensitive nanoparticles, compared with PtTPTBPF incorporated RL-100 polymer-based oxygen sensitive nanoparticles.

5.3 Energy transfer in the conjugated polymer-based oxygen-sensitive nanoparticles

As was described above, the efficient energy transfer from conjugated polymer to the (benzo)porphyrin was observed in the nanoparticles. The solutions of the conjugated polymers in organic solvents (uncharged polymer precursors in toluene) were further investigated.

Figure 5.5 Dissolved conjugated polymers (left) and conjugated polymer-based nanoparticles (right) under UV light.

The photography images of the toluene solution of a conjugated polyer incorporating PtTFPP in toluene and the dispersion of the positively charged nanoparticles in water (both anoxic) under excitation with a 365-nm line of the UV lamp,

The spectral difference of conjugated polymer and conjugated polymer-based nanoparticles can be seen by a naked eye under UV light (Figure 5.5.). It is evident that the energy transfer is very efficient in case of the nanoparticles (virtually no blue emission from the conjugated polymer is visible) but is absent in case of the dissolved polymer (emitting solely blue light). The spectra below (Figure 5.6.) confirm the above observation.

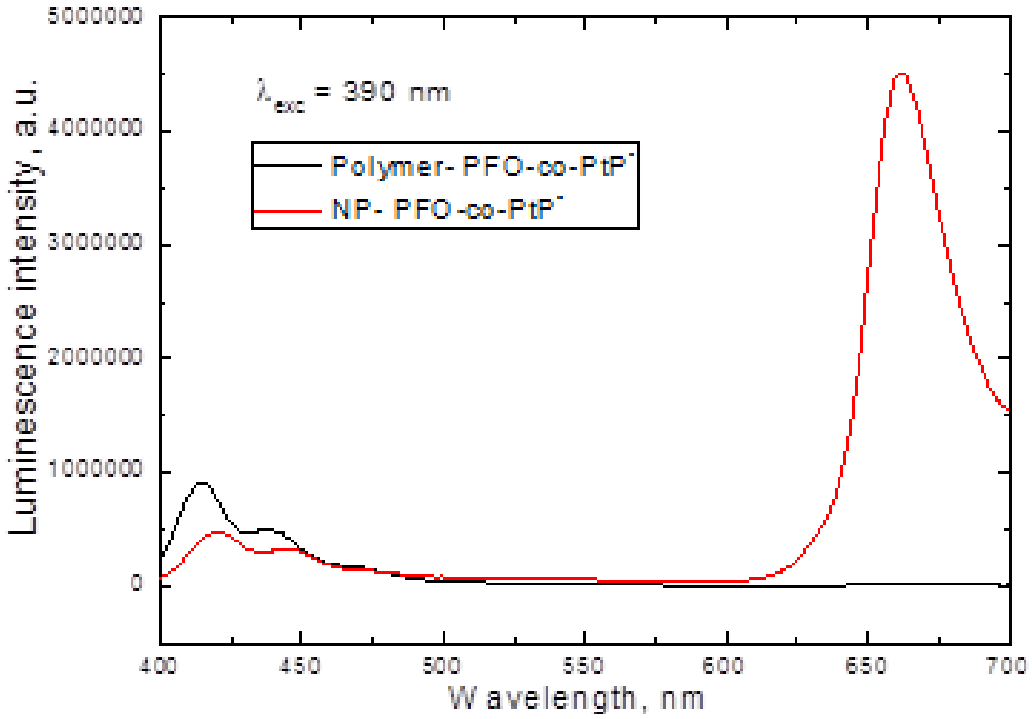

Figure 5.6. Emission spectra of dissolved PtTFPP integrated conjugated polymer and PtTFPP integrated conjugated polymer-based nanoparticles dispersion. (λ_{exc} = 390 nm)

We provide the following explanation for the above phenomenon. The conjugated polymer incorporating integrated PtTFPP has a long linear structure which is preserved in solution (Figure 5.6.). The energy transfer from the conjugated polymer to the porphrin is not efficient, as

the effective energy absorption radius cannot cover all conjugated polymer units. FRET mechanism is quite likely since the emission bands of the conjugated polymer and the absorption of the Q-bands of PtTFPP overlap. When the polymeric nanoparticles are formed, the distance between the energy donor conjugated polymer and the energy acceptor porphrin is significantly smaller. Thus, the more efficient energy transfer is realized in this nanoparticles form.

As observed from Figure 5.9. the same trends are observed for the NIR-emittting conjugated polymer incorporating Pt(II) benzoporphyrin. The same spectral properties are shown in PtTPTtBuBP system above. The oxygen indicator PtTPTBTPF can be excited at 615 nm and has emission at 770 nm wavelength. The corresponding conjugated polymer has excitation and emission wavelength at 460 nm and 550 nm respectively. Virtually no emission can be seen around 770 nm from PtTPTtBuBP integrated conjugated polymer in anoxic toluene solution. On the contrary, huge band at 770-780 nm is observed for the dispersion of PtTPTtBuBP integrated conjugated polymer-based nanoparticles.

Figure 5.7. Possible configuration of dissolved polymer

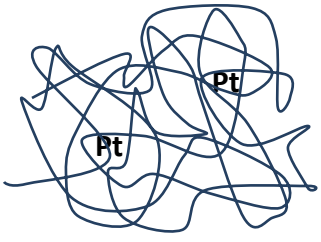

Figure 5.8. Possible configuration of nanoparticles

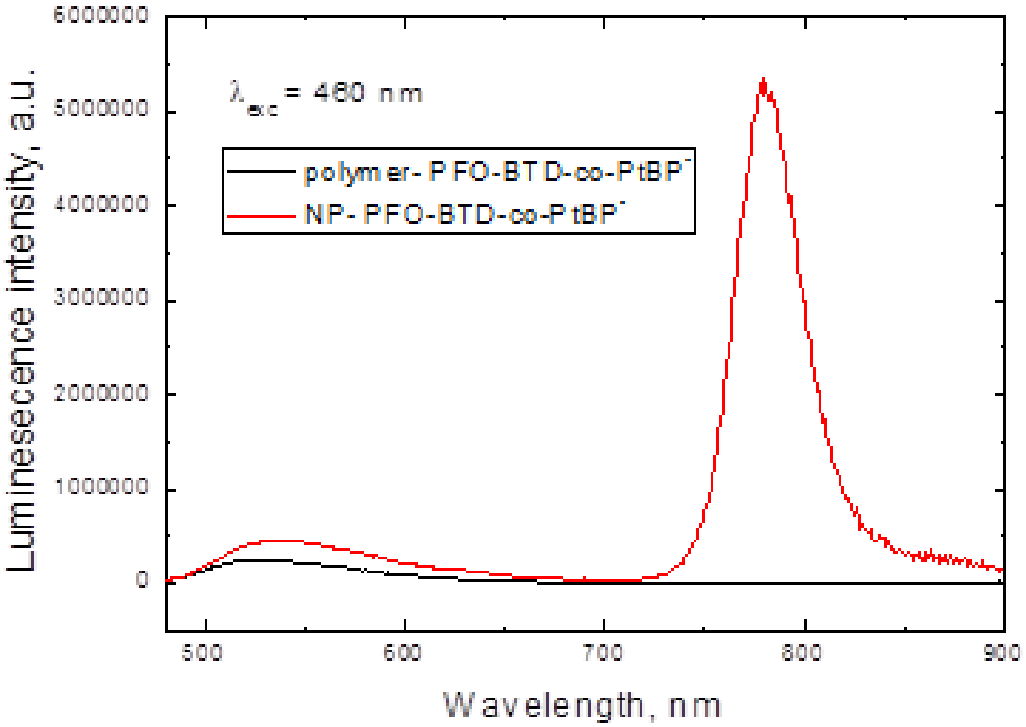

Figure 5.9. Emission spectra of dissolved PtTPTtBuBP integrated conjugated polymer and PtTPTtBuBP integrated conjugated polymer-based nanoparticles dispersion. (λexc = 460 nm)

5.4 Decay time of conjugated polymer-based oxygen-sensitive nanoparticles

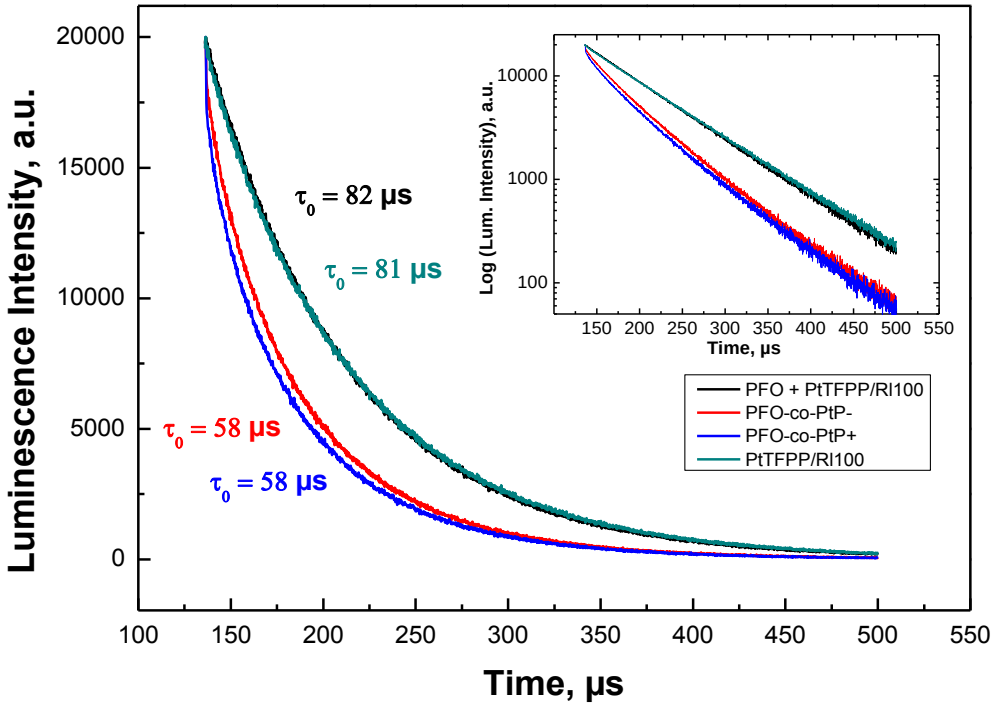

Figure 5.10. Luminescence decay of PtTFPP integrated conjugated polymer-based oxygen sensitive nanoparticles. (The insert shows the logarithmic plots. All measurements were done in deoxygenated dispersions.)

In this part, we compared the decay time of PtTFPP integrated conjugated polymer-based oxygen sensitive nanoparticles with PtTFPP-RL-100 nanoparticles and PFO-PtTFPP-RL-100 nanoparticles. For the PtTFPP system, data is fitted using a mono-exponential fit. The decay time for PtTFPP-RL-100 nanoparticles and PFO-PtTFPP-RL-100 nanoparticles are 81 μs and 82 μs, respectively. The decay time for cationic and anionic PtTFPP integrated conjugated polymer-based nanoparticles is

shorter (58 μs). This luminescence intensity decrease in conjugated polymer-based nanoparticles system may be due to the possible quenching of porphyrin phosphorescence by conjugated polymer. The energy of the triplet state of the conjugated polymers is lower than the energy level of porphrins. So if the porphrin is excited by the energy transferred from conjugated polymers, the emission may diminish due to further triplet-triplet energy transfer to the conjugated polymer. This can explain the shorter decay time of conjugated polymer-based oxygen-sensitive nanoparticles.

Similar trend is observed in case of the Pt(II)-benzoporphyrin-based conjugated polymer particles (Fig. ..). The shorter decay time has also been observed in PtTPTtBuBP integrated conjugated polymer-based nanoparticles than PtTPTBPF-RL-100 nanoparticles. The data of PtTPTtBuBP conjugated polymer-based nanoparticles are fitted in a two-exponential fit. The decay times of cationic conjugated polymer-based nanoparticles are 41 μs and 15 μs, with the intensity of 83 % and 17 % respectively. For anionic conjugated polymer-based nanoparticles are 40 μs and 14 μs, with the intensity of 82 % and 18 % respectively. On the other hand, the decay profile of PFO-PtTPTBPF-RL-100 nanoparticles is excellently fitted in a mono-exponential fit (τ = 61 μs). The same explanation for PtTFPP system can also be applied here.

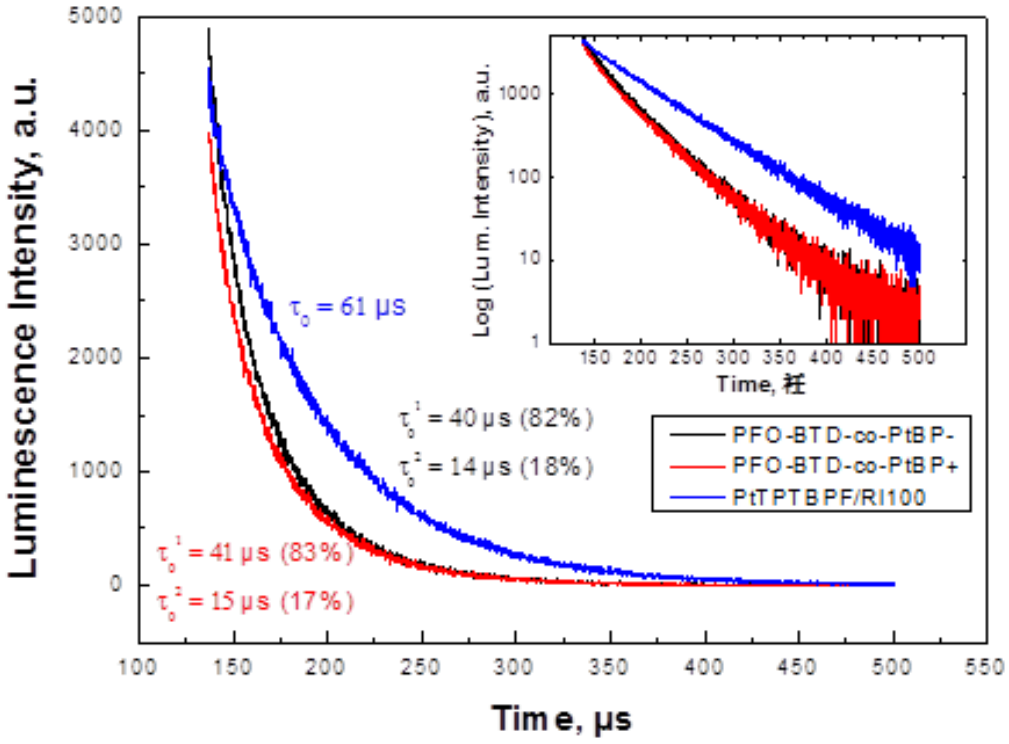

Figure 5.11. Luminescence decay of PtTPTtBuBP integrated conjugated polymer-based oxygen sensitive nanoparticles. (The insert shows the logarithmic plots. All measurements were done in deoxygenated dispersions.)

5.5 Oxygen sensitivity of the conjugated polymer-based oxygen-sensitive nanoparticles

The mechanism of oxygen sensors is based on the dynamic quenching of the indicator's luminescence by molecular oxygen. So we compared the spectra of PtTFPP integrated conjugated polymer-based oxygen sensor and PtTPTtBuBP integrated conjugated polymer-based oxygen sensor when they are exposed in air and when deoxygenated.

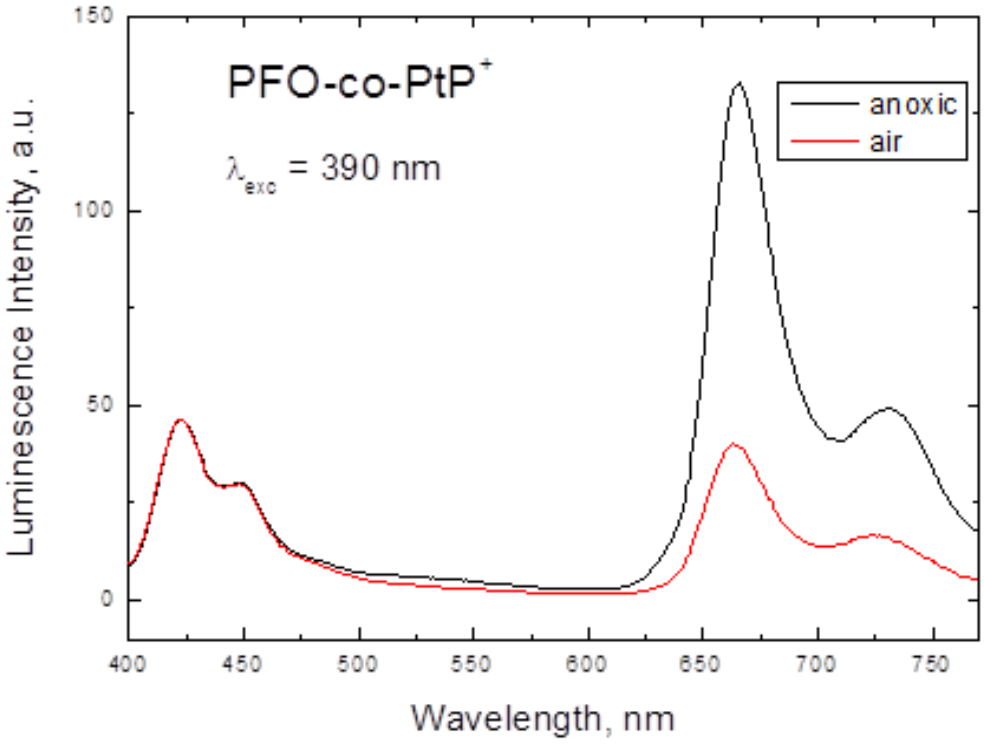

Figure 5.12. Emission spectra of PtTFPP integrated conjugated polymer-based nanoparticle under air saturation and under anoxia condition

For PtTFPP integrated conjugated polymer-based nanoparticle oxygen sensor, we excited it at 390 nm wavelength, which is optimal for conjugated polymer. One can see (Figure 5.12.) that luminescence intensity of this oxygen sensor at deoxygenated condition is 3 – 4 times higher than saturated in air. Importantly, the residual blue emission from the conjugated polymer is not affected. Thus, the system is suitable for ratiometric 2-wavelength measurement.

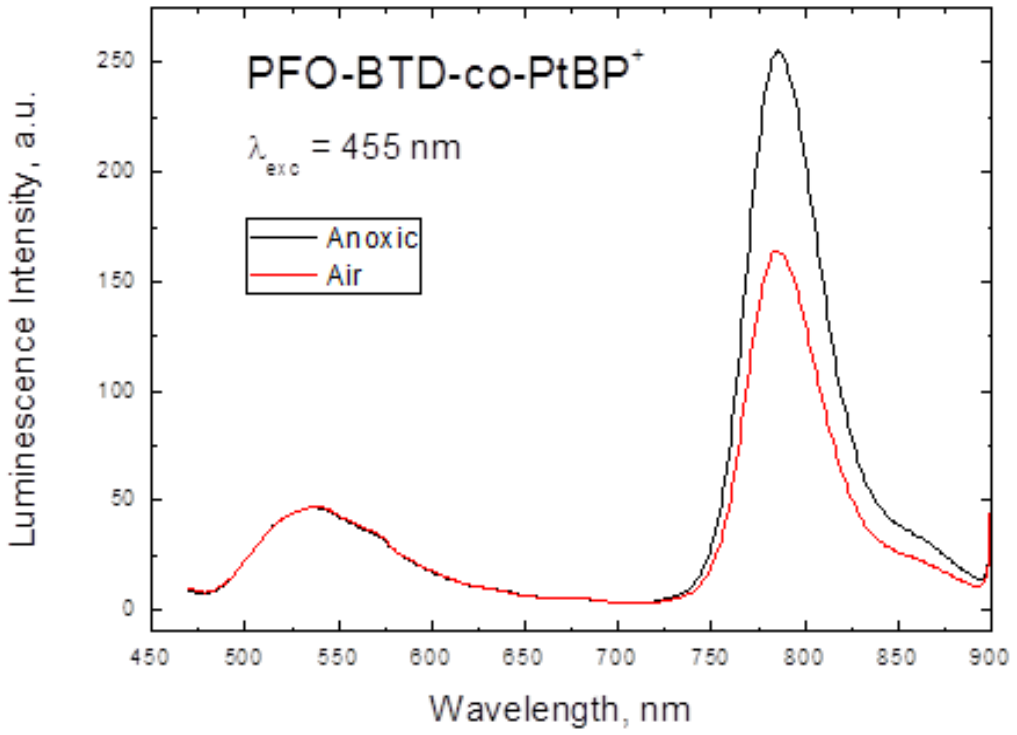

Figure 5.13. Emission spectra of PtTPTtBuBP integrated conjugated polymer-based nanoparticle under air saturation and under anoxia condition

The Pt(II) benzoporphyrin-integrated conjugated polymer nanoparticles show similar behaviour (Figure 5.13.). However, the sensitivity is significantly lower than for the PtTFFPP-integrated polymer beads. This is partly due to shorter decay time of the Pt(II) benzoporphyrin, but is also

likely that the morphology of the particles is more important here. In fact, the PtTFPP-beads can only be connected twice with the conjugated polymer. On the other side, up to 4 bonds are possible for PtTPTtBuBP. Thus, the conjugated polymer chains may better shield the oxygen indicator from the quencher.

5.6 Particles properties of conjugated polymer-based oxygen-sensitive nanoparticles

Some other characterizations have been done for these 2 categories, 5 kinds of conjugated polymer based luminescent oxygen sensitive nanoparticles were investigated.

Table 5.1. Particles properties of conjugated polymer-based oxygen-sensitive nanoparticles

	Z-Ave (d.nm)	Pdl	ZP (mV)
PFO-co-PtP^{+}	35.17	0.249	33.5
PFO-co-PtP^{-}	55.58	0.192	-23.1
PFO-co-PtP$^{+/-}$	37.41	0.192	22.5
PFO-BTD-co-PtBP^{+}	51.78	0.129	33
PFO-BTD-co-PtBP^{-}	49.75	0.094	-23.2

All of these oxygen sensors have small particle size, which is around or below 50 nm. It shows ability for cell penetrating in biological application. Small Pdl value shows the oxygen sensor particle are quite homogenous in size. Cationic and anionic sensors show positive and negative charges on the particles surface, respectively, which explains their good dispersability in water and ability to interact with different kinds of microorganism. As can be seen, the Zeta-potential of the particles is dependent on the nature of the charged group and is not dependent on the nature of the porphyrin incorporated.

Interestingly, the zeta-potential of zwitterionic conjugated polymer-based nanoparticles is positive. During the synthesis process, we have both positive and negative charged monomers involved. For some reason, the positive charged group is dominant after the nanoparticles synthesis. More study could be done for these "zwitterionic" conjugated polymer-based nanoparticles in real biological system to see the difference with conventional cationic and anionic ones.

5.7 Cell penetration ability of conjugated polymer-based oxygen-sensitive nanoparticles

Cell penetration of the particles was investigated by incubating the MEF cells with 10 μg/mL dispersion of the beads for 18h. As can be seen Figure 5.14., the cationc and anionic particles containing copolymerized PtTFPP show excellent uptake by the cells. These particles can be particularly promising for ratiometric imaging of intracellular oxygen. On the contrary, the anionic conjugated polymer particles were shown to remain outside the MEF cells and can be

suitable for extracellular imaging of oxygen. The more detailed studies with MEF and other cell cultures are ongoing in the group of Prof. Dmitri Papkovsky in the University College Cork (Ireland).

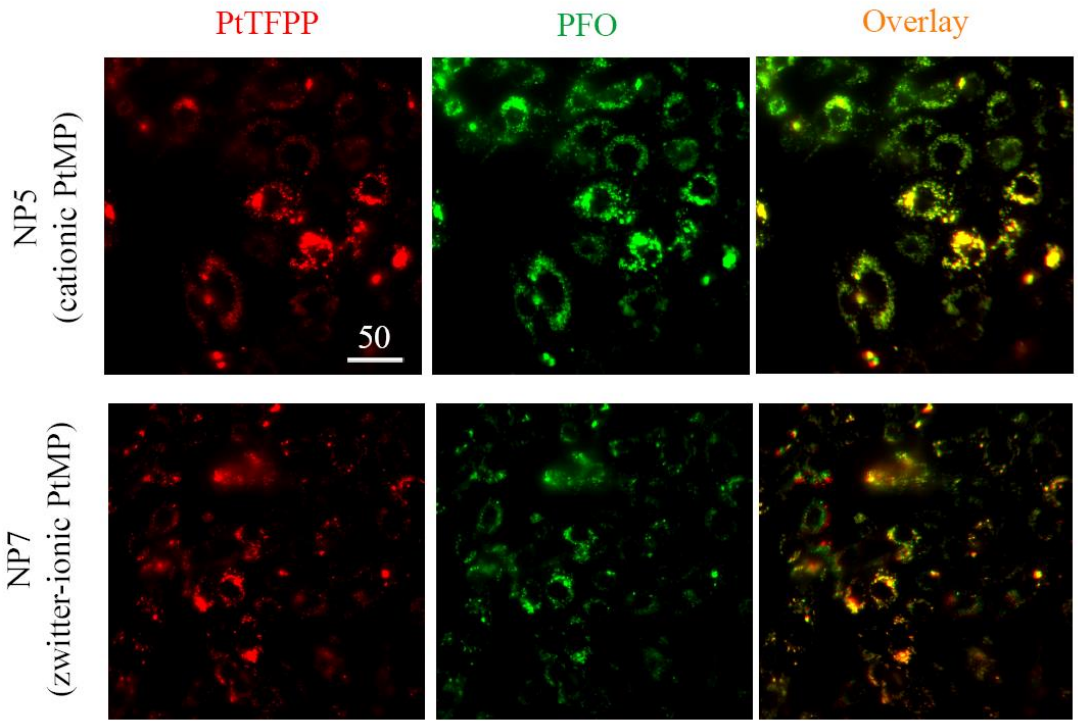

Figure 5.14. Microscopic images of the MEF cells incubated with the cationic and zwitterionic conjugated polymer particles

The oxygen-sensing properties inside the cells and applications are currently investigated together with cooperation partners.

6 Conclusions

In conclusion, this series of conjugated polymer-based oxygen-sensitive nanoparticles were synthesized successfully. The synthetic methodology to incorporate charged functionalities and oxygen-sensitive indicator is established by zeta potential measurement and sir-saturated/ anoxic condition emission excitation spectrum. Conjugated polymers were synthesized by Suzuki coupling, and nanoparticles were prepared through fast precipitate method. All the particles are well dispersible in water.

Efficient energy transfer in particles in contrast to the dissolved polymers was established. Very high brightness, significant enhancement compared to the state-of-the-art beads is observed.

The luminescence of the new nanoparticles is sensitive to oxygen so that they are promising as oxygen-sensitive nano-probes. Also this series optical oxygen sensors are suitable for two-wavelength ratiometric sensing and imaging. Cationic and “zwitterionic” conjugated polymer-based oxygen-sensitive nanoparticles show the ability to penetrate the cells. It is the first time that NIR emitting beads are prepared. They are expected to be particularly promising for tissue applications.

7 References

1. Tripathi, M.M., et al., *An optical sensor for multi-species impurity monitoring in hydrogen fuel.* Sensors and Actuators B: Chemical, 2012. **171**: p. 416-422.
2. John, G.T., et al., *Integrated optical sensing of dissolved oxygen in microtiter plates: a novel tool for microbial cultivation.* Biotechnology and bioengineering, 2003. **81**(7): p. 829-836.
3. Wolfbeis, O.S., *Fiber optic chemical sensors and biosensors*. Vol. 1. 1991: CRC press Boca Raton, FL.
4. Nei, L. and R.G. Compton, *An improved Clark-type galvanic sensor for dissolved oxygen.* Sensors and Actuators B: Chemical, 1996. **30**(2): p. 83-87.
5. Amao, Y., *Probes and polymers for optical sensing of oxygen.* Microchimica Acta, 2003. **143**(1): p. 1-12.
6. Freeman, T.M. and W.R. Seitz, *Oxygen probe based on tetrakis (alkylamino) ethylene chemiluminescence.* Analytical chemistry, 1981. **53**(1): p. 98-102.
7. Wolfbeis, O.S., et al., *Fiber-optic fluorosensor for oxygen and carbon dioxide.* Analytical chemistry, 1988. **60**(19): p. 2028-2030.
8. Skoog, D., D. West, and F. Holler, *Fundamentals of Analytical Chemistry (5th edn.) Saunders College.* New York, 1988.
9. McDonagh, C., C.S. Burke, and B.D. MacCraith, *Optical chemical sensors.* Chemical reviews, 2008. **108**(2): p. 400-422.
10. Quaranta, M., S. Borisov, and I. Klimant, *Indicators for optical oxygen sensors.* Bioanalytical Reviews, 2012. **4**(2-4): p. 115-157.
11. Lee, Y.-E.K., R. Kopelman, and R. Smith, *Nanoparticle PEBBLE sensors in live cells and in vivo.* Annual review of analytical chemistry (Palo Alto, Calif.), 2009. **2**: p. 57.
12. Fercher, A., et al., *Intracellular O2 sensing probe based on cell-penetrating phosphorescent nanoparticles.* Acs Nano, 2011. **5**(7): p. 5499-5508.
13. Xu, H., et al., *A real-time ratiometric method for the determination of molecular oxygen inside living cells using sol-gel-based spherical optical nanosensors with applications to rat C6 glioma.* Analytical chemistry, 2001. **73**(17): p. 4124-4133.
14. Wu, C., et al., *Ratiometric single-nanoparticle oxygen sensors for biological imaging.* Angewandte Chemie, 2009. **48**(15): p. 2741-5.
15. Koo Lee, Y.-E., et al., *Near infrared luminescent oxygen nanosensors with nanoparticle matrix tailored sensitivity.* Analytical chemistry, 2010. **82**(20): p. 8446-8455.
16. Kondrashina, A.V., et al., *A Phosphorescent Nanoparticle-Based Probe for Sensing and Imaging of (Intra)Cellular Oxygen in Multiple Detection Modalities.* Advanced Functional Materials, 2012. **22**(23): p. 4931-4939.
17. Coogan, M.P., et al., *Probing intracellular oxygen by quenched phosphorescence lifetimes of nanoparticles containing polyacrylamide-embedded [Ru (dpp (SO3Na) 2) 3] Cl2.* Photochemical & photobiological sciences, 2010. **9**(1): p. 103-109.
18. Valeur, B. and M.N. Berberan-Santos, *Molecular fluorescence: principles and applications*2013: John Wiley & Sons.

19. So, P.T., et al., *Two-photon excitation fluorescence microscopy.* Annual review of biomedical engineering, 2000. **2**(1): p. 399-429.
20. Blum, L.J. and L. Blum, *Bio-and chemi-luminescent sensors*1997: World Scientific.
21. Gründler, P., *Chemical sensors: an introduction for scientists and engineers*2007: Springer.
22. Borisov, S.M. and O.S. Wolfbeis, *Optical biosensors.* Chemical reviews, 2008. **108**(2): p. 423-461.
23. Tang, B., et al., *A near-infrared neutral pH fluorescent probe for monitoring minor pH changes: imaging in living HepG2 and HL-7702 cells.* Journal of the American Chemical Society, 2009. **131**(8): p. 3016-3023.
24. Larsen, M., et al., *A simple and inexpensive high resolution color ratiometric planar optode imaging approach: application to oxygen and pH sensing.* Limnol. Oceanogr.: Methods, 2011. **9**: p. 348-360.
25. Arain, S., et al., *Characterization of microtiterplates with integrated optical sensors for oxygen and pH, and their applications to enzyme activity screening, respirometry, and toxicological assays.* Sensors and Actuators B: Chemical, 2006. **113**(2): p. 639-648.
26. Schouest, K., et al., *Toxicological assessment of chemicals using Caenorhabditis elegans and optical oxygen respirometry.* Environmental toxicology and chemistry, 2009. **28**(4): p. 791-799.
27. Mills, A., *Oxygen indicators and intelligent inks for packaging food.* Chemical Society Reviews, 2005. **34**(12): p. 1003-1011.
28. Nagl, S. and O.S. Wolfbeis, *Classification of chemical sensors and biosensors based on fluorescence and phosphorescence,* in *Standardization and Quality Assurance in Fluorescence Measurements I*2008, Springer. p. 325-346.
29. Baldini, F., et al., *Optical chemical sensors*. Vol. 224. 2006: Springer.
30. Lobnik, A., et al., *pH optical sensors based on sol–gels: chemical doping versus covalent immobilization.* Analytica chimica acta, 1998. **367**(1): p. 159-165.
31. Wang, X.-D. and O.S. Wolfbeis, *Fiber-optic chemical sensors and biosensors (2008–2012).* Analytical chemistry, 2012. **85**(2): p. 487-508.
32. Carraway, E., et al., *Photophysics and photochemistry of oxygen sensors based on luminescent transition-metal complexes.* Analytical chemistry, 1991. **63**(4): p. 337-342.
33. Dunphy, I., S.A. Vinogradov, and D.F. Wilson, *Oxyphor R2 and G2: phosphors for measuring oxygen by oxygen-dependent quenching of phosphorescence.* Analytical biochemistry, 2002. **310**(2): p. 191-198.
34. Vogel, A. and V. Venugopalan, *Mechanisms of pulsed laser ablation of biological tissues.* Chemical reviews, 2003. **103**(2): p. 577-644.
35. Patil, A., A. Heeger, and F. Wudl, *Optical properties of conducting polymers.* Chemical reviews, 1988. **88**(1): p. 183-200.
36. Kajzar, F., et al., *< i> X</i>< sup>(3)</sup> of trans-(CH)< sub> x</sub>: Experimental observation of 2A< sub> g</sub> excited state.* Synthetic Metals, 1987. **17**(1): p. 563-567.
37. Schmitt-Rink, S., D. Miller, and D.S. Chemla, *Theory of the linear and nonlinear optical properties of semiconductor microcrystallites.* Physical Review B, 1987. **35**(15): p. 8113.
38. Marder, S.R., J.E. Sohn, and G.D. Stucky, *Materials for Nonlinear Optics Chemical Perspectives*, 1991, DTIC Document.

39. Sailor, M.J., et al., *Thin films of n-Si/poly-(CH3) 3Si-cyclooctatetraene: conducting-polymer solar cells and layered structures.* Science, 1990. **249**(4973): p. 1146-1149.
40. Burroughes, J., et al., *Light-emitting diodes based on conjugated polymers.* nature, 1990. **347**(6293): p. 539-541.
41. Bradley, D., *Conjugated polymer electroluminescence.* Synthetic Metals, 1993. **54**(1): p. 401-415.
42. McQuade, D.T., A.E. Pullen, and T.M. Swager, *Conjugated polymer-based chemical sensors.* Chemical reviews, 2000. **100**(7): p. 2537-2574.
43. Borisov, S.M., et al., *Precipitation as a simple and versatile method for preparation of optical nanochemosensors.* Talanta, 2009. **79**(5): p. 1322-1330.
44. Buck, S.M., et al., *Optochemical nanosensor PEBBLEs: photonic explorers for bioanalysis with biologically localized embedding.* Current opinion in chemical biology, 2004. **8**(5): p. 540-546.
45. Dmitriev, R.I., et al., *Assessment of cellular oxygen gradients with a panel of phosphorescent oxygen-sensitive probes.* Analytical chemistry, 2012. **84**(6): p. 2930-2938.
46. Pu, K.Y., Z. Fang, and B. Liu, *Effect of charge density on energy ‐transfer properties of cationic conjugated polymers.* Advanced Functional Materials, 2008. **18**(8): p. 1321-1328.

8 list of tables

9 list of figures